Sequence and relative timing of large lakes in Gale crater (Mars) after the formation of Mount Sharp

Marisa Palucis, William Dietrich, Rebecca Williams, Alexander Hayes, Tim Parker, Dawn Sumner, Nicolas Mangold, Kevin Lewis, Horton Newsom

AGU PUBLICATIONS

JGR

Journal of Geophysical Research: Planets

RESEARCH ARTICLE
10.1002/2015JE004905

Key Points:
- Delta deposits within Gale suggest a series of lake stands post-Mount Sharp development
- Incisional and depositional processes record a sequence of falling then rising lake levels
- Water supply for lakes likely shifted from a regional to more local source over time

Supporting Information:
- Figures S1–S8 and Tables S1–S4

Correspondence to:
M. C. Palucis,
mpalucis@caltech.edu

Citation:
Palucis, M. C., W. E. Dietrich, R. M. E. Williams, A. G. Hayes, T. Parker, D. Y. Sumner, N. Mangold, K. Lewis, and H. Newsom (2016), Sequence and relative timing of large lakes in Gale crater (Mars) after the formation of Mount Sharp, *J. Geophys. Res. Planets*, *121*, 472–496, doi:10.1002/2015JE004905.

Received 21 JUL 2015
Accepted 23 FEB 2016
Accepted article online 1 MAR 2016
Published online 30 MAR 2016

Sequence and relative timing of large lakes in Gale crater (Mars) after the formation of Mount Sharp

Marisa C. Palucis[1], William E. Dietrich[2], Rebecca M. E. Williams[3], Alexander G. Hayes[4], Tim Parker[5], Dawn Y. Sumner[6], Nicolas Mangold[7], Kevin Lewis[8], and Horton Newsom[9]

[1]Division of Geological and Planetary Sciences, California Institute of Technology, Pasadena, California, USA, [2]Department of Earth and Planetary Science, University of California, Berkeley, California, USA, [3]Planetary Science Institute, Tuscan, Arizona, USA, [4]Department of Astronomy, Cornell University, Ithaca, New York, USA, [5]NASA Jet Propulsion Laboratory, California Institute of Technology, Pasadena, California, USA, [6]Geology Department, University of California, Davis, California, USA, [7]Laboratoire Planetologie et Geodynamique de Nantes, LPGN/CNRS UMR6112, Universite de Nantes, Nantes, France, [8]Department of Earth and Planetary Sciences, The Johns Hopkins University, Baltimore, Maryland, USA, [9]Institute of Meteoritics, University of New Mexico, Albuquerque, New Mexico, USA

Abstract The quantification of lake levels in Gale crater is important to define the hydrologic and climatic history experienced by the sedimentary deposits found by *Curiosity*. We propose that there were at least three major lake stands within Gale, each persisted >1000 years, and all occurred after Mount Sharp reached close to its current topographic form. Deltaic deposits off the southern rim of Gale, derived from incision of Farah Vallis, and corresponding deposits off the southern flank of Mount Sharp define the highest lake level, which had a mean depth of 700 m. Canyons similar in form to Farah Vallis enter into craters and/or the crustal dichotomy near Gale from the south, suggesting that the highest lake was supplied by a large-scale flow system. The next lake level, established after a period of drying and rewetting, is defined by four deltaic features, three sourced from Mount Sharp and one from the western rim of Gale, as well as the termination of gullies around the northern rim of Gale. This second lake level had a mean depth of 300 m. The presence of the gullies suggests more locally sourced water. Lake levels then rose another 100 m, as evidenced by two deltaic deposits derived from the rim of Gale and the termination of a second set of gullies. Post-lake, reduced hydrologic activity continued, evidenced by a time of fan building (including Peace Vallis). The sequence of events suggests an episodic shift through time from relatively wet regional conditions to a drier environment with local runoff.

1. Introduction

Orbital imagery suggests that lakes may have once existed on the surface of Mars [e.g., *Cabrol and Grin*, 2010]. The Mars Science Laboratory (MSL) rover, *Curiosity*, which landed in Gale crater, a Late Noachian to Early Hesperian-aged crater [*Thomson et al*., 2011], allows us to directly test the hypothesis that Mars's past climate was able to support large lakes. The rover's landing ellipse contained the distal end of the Peace Vallis alluvial fan [*Anderson and Bell*, 2010; *Palucis et al*., 2014], where fine-grained sedimentary rocks were found and inferred to represent an ancient lake during the post-Noachian period of Mars [*Grotzinger et al*., 2014]. Over its traverse from the landing site to the base of Aeolis Mons (informally Mount Sharp), a 5 km high mound showing a distinct mineralogical transition from phyllosilicates to sulfates [*Milliken et al*., 2010], *Curiosity* studied dozens of outcrops, collecting image data for grain size, texture, and strata geometry. Based on these data, *Grotzinger et al*. [2015] concluded that these outcrops were fluvial, deltaic, and lacustrine in origin and that this crater-lake system lasted thousands to millions of years, depositing sediments that were presumably later exhumed by wind erosion [*Malin and Edgett*, 2000] to form the lower base of Aeolis Mons (possibly the lowest 75 to 250 m of sediment). But Gale crater also hosts a number of morphologic features suggestive of crater-wide gullying and lacustrine activity post-Aeolis Mons. These include (Figure 1): well-defined incised valleys and valley networks around the crater rim, including a large canyon entering Gale from the south (Farah Vallis), deltaic and fan deposits, and channels (both regular and inverted) [*Cabrol and Grin*, 1999; *Pelkey et al*., 2004; *Irwin et al*., 2005; *Anderson and Bell*, 2010; *Dietrich et al*., 2013, 2014; *Le Deit et al*., 2013; *Palucis et al*., 2014].

The Gale-forming impact occurred on the crustal dichotomy of Mars, and as observed by *Irwin et al*. [2005], ejecta from the impact partially buried a valley network originating near Herschel crater to the South [see

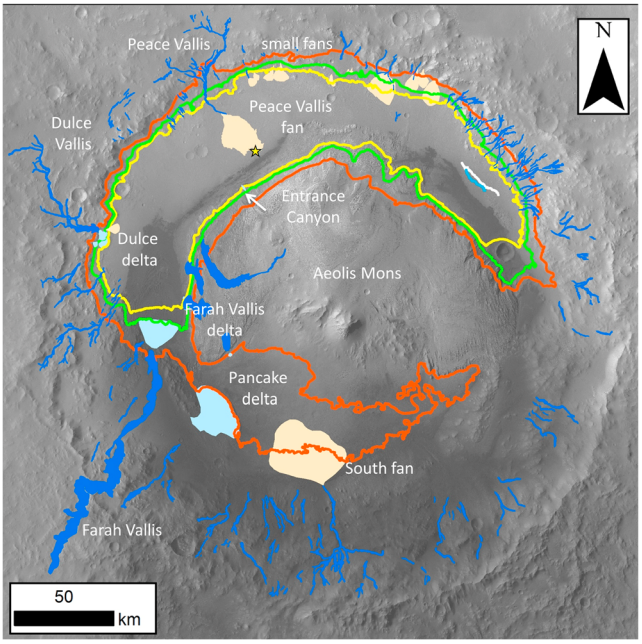

Figure 1. A modified version of the geomorphic map from *Anderson and Bell* [2010] showing their map of "valleys and canyons" (dark blue) and the Peace Vallis fan, where the MSL landing site has been marked with a star. Several large fans (tan) and deltas (light blue) were added to their map and are discussed in detail within the text. The inferred paleolake stands are shown, which correspond to the −3280 m HRSC contour (Pancake lake stand, orange), the −3780 m HRSC contour (Farah Vallis lake stand, green), and the −3980 m HRSC contour (Dulce Vallis lake stand, yellow).

Irwin et al., 2005, Figure 4], which *Irwin et al*. [2005] point to as evidence that the network was active prior to Gale's formation. They hypothesized that this extensive regional drainage system provided the water needed to incise Farah Vallis and support lake and delta formation, but not by a reestablished channel system. Instead, subsurface flow was important. They also suggested that this period of lake building occurred after Mount Sharp sediments were deposited and partially removed by aeolian erosion [*Malin and Edgett*, 2000]. Others have also proposed large lakes in Gale (see review in *Anderson and Bell* [2010]; *Cabrol et al*. [1999]; *Le Deit et al*. [2013]; *Fairen et al*. [2014]; and *Dietrich et al*. [2013, 2014]). The timing, extent, and duration of these lakes, though important to climate reconstructions and the water inundation history (and possible diagenetic influence) of the sediments being studied along Curiosity's traverse, are unknown.

Here we exploit orbital imagery and photogrammetrically derived digital elevation data to document distinct lake levels that occupied large portions of Gale crater after the formation of Mount Sharp. We first identify and describe in detail several deposits sourced either from the rim of Gale crater or from Mount Sharp deposits. Based on the topography of these deposits, we interpret them to be deltaic deposits, and for each we compare the eroded volume of material from valley/canyon incision to the volume of the deposit. This analysis constrains the source of sediment (and water) to build these deposits and places bounds on the extent of preservation of the deposits and the applicability of using them to infer past lake levels. From our observations, we then propose a clear sequence of lake level decline followed by lake level rise, as well as changes in the relative contribution of regional versus local water sources, a substantial refinement of our understanding of the lacustrine history at Gale crater. We then use our topographic analysis to constrain the hydrologic conditions driving lake level dynamics and propose a probable hydrogeomorphic sequence of events from the time of Gale's impact to present day.

2. Methodology

2.1. Topographic Data

Most of the analyses presented here (Table S1 in the supporting information) used either a HIRISE (High Resolution Imaging Science Experiment) topographic data set (1 m/pixel post spacing, 0.25 m/pixel imagery, red box in Figure 2) or a HRSC (High Resolution Stereo Camera) topographic data set (50 m post spacing, covers the entire extent of Figure 2), both provided to the MSL team. A complete list of the HIRISE and HRSC stereopairs and images used to make the digital elevation models (DEMs) and orthophotos is listed in Table 4 in *Golombek et al*. [2012]. In addition to these DEMs, we created several 18 m resolution topographic data sets using CTX (Context Camera) stereo images. We had 16 to 20 tie points spread throughout the DEM boundary, and the tie points were given *z* control (elevation) using the Mars Orbiter Laser Altimeter (MOLA) DEM. The CTX DEMs were created to improve upon the MSL-provided HRSC DEM in performing topographic analyses of several of the delta and smaller fan features within Gale crater (black boxes in Figure 2). For consistency throughout the paper, the HRSC-derived elevation will be reported for each delta front. Depending on the

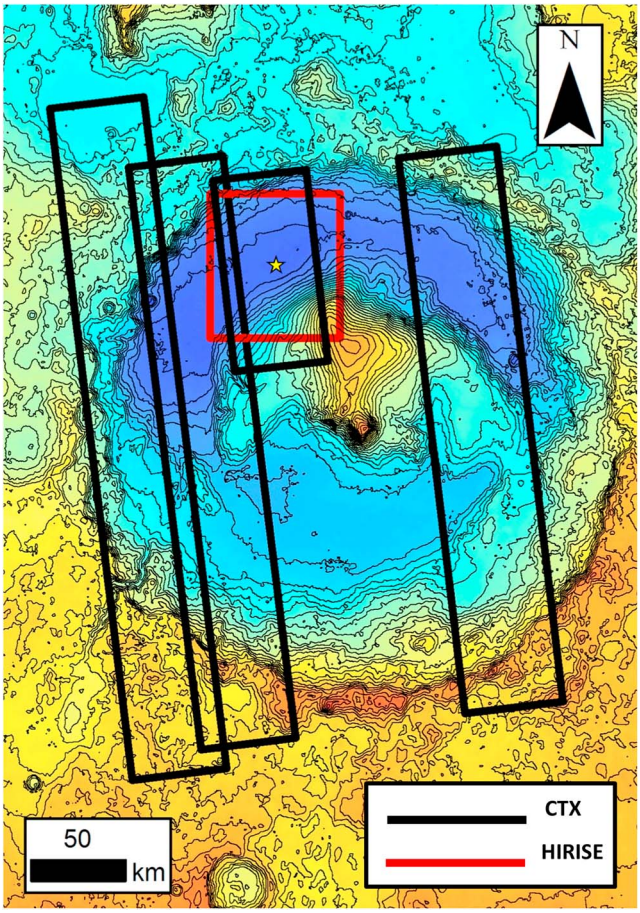

Figure 2. An HRSC elevation map of Gale crater with 200 m HRSC contours. The areas for which we have made CTX DEMs are outlined in black. The region where HIRISE coverage is available is outlined in red. The CTX DEM near the landing site (marked with a star) was provided by the MSL project, while the remaining CTX DEMs were created using CTX stereo pairs (G05_020265_1746_XI_05S223W/G04_019843_1746_XI_05S223W, B21_017786_1746_XN_05S222W/P04_002675_1746_XI_05S222W, and F04_037407_1745_XN_05S221W/P19_008437_1746_XN_05S221W) and the commercial software SOCET SET. The star marks the location of *Curiosity*'s landing (i.e., Bradbury Rise). The eastern and western "flanks" of Aeolis Mons are also shown.

various data sets used (i.e., HIRISE versus CTX DEMs), the contour line values are ±20 m within the HRSC values.

2.2. Volume Calculations

Much of the topographic analysis presented here relies on Geographic Information Systems (GIS) methods similar to those developed by *Warner et al*. [2011] for basin and lake volumes. In brief, we digitized the topography of the margins of the proposed lake level or incised valley and assigned an elevation to each rim data point from the base DEM. We then constructed a triangulated irregular network (TIN) across the valley or lake to represent either the original, uneroded topography or the lake surface. The TIN was then converted to a gridded raster, and this raster was differenced from the base DEM to obtain a volume (the depth at each grid cell is also calculated). In some of the source areas, the topographic data were limited in extent or were too coarse to resolve the smaller channels higher up in the drainage network. In these cases, we followed the methodology described in *Palucis et al*. [2014] for calculating erosional volumes.

To estimate delta deposit volumes, we used two methodologies. When possible, we first eliminated the delta form (mapped in planform) and projected the nearby local topography (typically the crater wall or floor) laterally under the area occupied by the delta feature to create a pre–delta surface. We then took the difference between the gridded delta surface and this projected pre–delta surface to estimate the volume of the delta. This methodology is described in detail for the Peace Vallis fan in *Palucis et al*. [2014]. Due to the complexity of re-creating the local topography in some regions, in these locations we constructed several long profiles (typically 5–10 profiles depending on the planform area of the delta) down each delta feature and out onto the floor it built upon. For each profile we then projected the slope of the floor linearly back upslope under the delta deposit and determined the depth of the deposit. This depth was then applied to the entire segment (each segment is one half the distance to the long profile to the right plus one half the distance to the long profile to the left) to determine the segment volume. The segment volumes were summed to get the total delta volume. On one delta we tested both methods and got comparable results (1.4 km^3 for a complete topographic reconstruction and 1.5 km^3 using five long profiles). We assume in our analysis that since the source material for the deltaic deposits is mostly granular deposits of colluvium, dust, ejecta, and brecciated rock from the impact, rather than intact bedrock, the bulk density of the eroded and deposited material is approximately the same, such that volumes can be directly compared. Our methodology used ArcGIS tools, though all postprocessing was conducted in MATLAB.

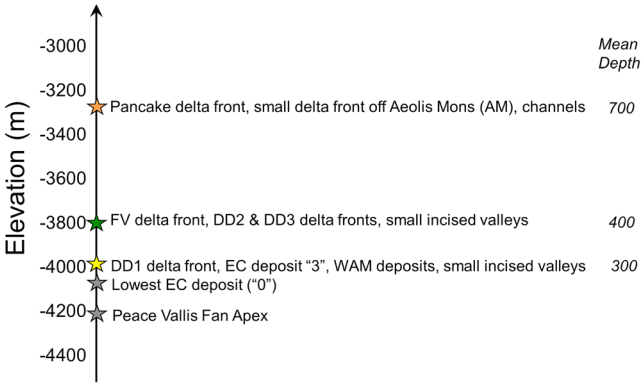

Figure 3. A semigraphical representation of the geomorphic features identified herein and their elevation (in meters, based on HRSC DEM data), which we use to define three distinct lake stands within Gale crater. The orange star marks the −3280 m stand, the green star marks the −3780 m stand, and the yellow star marks the −3980 m stand. Features corresponding to a lake stand are listed to the right of the colored stars, and the mean depth of the stand is shown in the right-hand column. Other geomorphic features of interest (e.g., the Peace Vallis fan) are also shown. For reference, FV = Farah Vallis, DD = Dulce Deposits, EC = Entrance Canyon deposits, and WAM = Western Aeolis Mons deposits.

2.3. Crater Counting

We counted the density of impact craters on Gale's lower inner walls and floor (defined as being areas within the crater rim that have slopes less than ~5°—the lower walls typically have slopes between 2 and 5° and the floor is typically <2°—and excluding Mount Sharp deposits) by mapping onto CTX imagery in ArcGIS using CraterTools software [*Kneissl et al.*, 2011]. In order to compare differences in a region's ability to retain craters, we mapped all craters within Gale's wall and floor, acknowledging that we may have included some secondary craters in our count. In general, the resolution of the CTX data enabled us to map craters down to ~12 m in diameter. We extracted crater area, and hence crater diameter, from our maps to compile crater frequency plots in Craterstats II [*Michael and Neukum*, 2010] using (a) the *Hartmann* [2005] chronology and production functions with root-2 bins and (b) the *Ivanov* [2001] production function and *Hartmann and Neukum* [2001] chronology function with pseudo-log bins. Both approaches are presented, as both *Hartmann* [2005] and *Hartmann and Neukum* [2001] acknowledge greater uncertainties in the middle period of Martian history.

3. Observations: Delta, Fan and Channel Deposits Within Gale Crater

Across Gale there are several large depositional features with arcuate forms emanating from or associated with incised valleys. The basic architecture of these features is that they have gently sloping tops that transition to a steeply dipping front that then merges with the topography of the basin into which these features formed. *Gilbert* [1890] first described in detail the same form on Earth, now referred to as a Gilbert delta, which results from a river encountering a still body of water (e.g., a lake). In the following sections we describe several features within Gale that follow this morphological form, which we infer to be delta features. For simplicity, we will refer to them as delta deposits throughout the text, but they are all hypothesized delta deposits, as we lack sedimentological data for these features at present. Depositional landforms denoted by convex contours relative to their background walls and lacking a sharp break in slope at their distal ends are mapped as alluvial fans and are also documented, as they indicate additional periods of hydrologic activity within Gale.

Figure 3 plots depositional features as a function of elevation. Below we describe these features, which later provide the basis for our interpretation that they record a sequence of lake stands in Gale (sections 4–6). The elevation correspondence at the same level of several deposits and valleys and channels supports the lake interpretation and makes it unlikely that the distal end of these features experienced significant upslope erosional retreat since formation. Our analysis suggests that the levels neither systematically declined nor rose, but instead, we find evidence for multiple rise and fall events.

3.1. The Farah Vallis-Pancake Delta and Farah Vallis Delta-Fan Systems

The Farah Vallis ("FV" in Figure 3) system consists of a source canyon followed downstream first by a fan then, after further incision, a delta deposit. On this delta deposit lays a second thin small fan that was subsequently deposited. Sediment from Farah Vallis was also transported east to the aerially largest, and perhaps best-preserved, delta (i.e., the Pancake Delta) in Gale (Figures 4 and S1). We describe this system in detail herein.

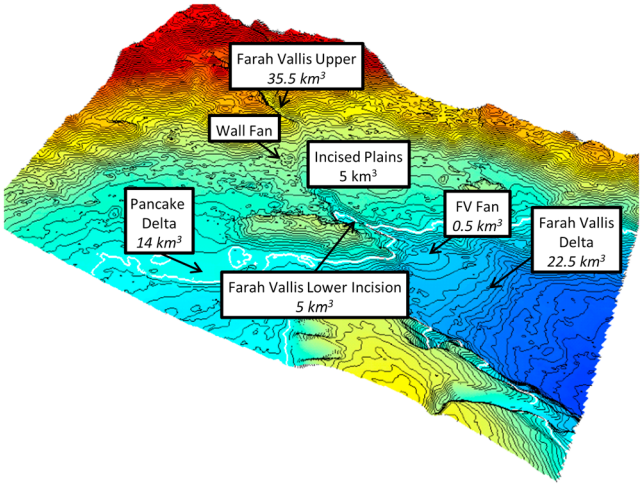

Figure 4. A three-dimensional view of the Farah Vallis system looking southwest (vertical exaggeration of 1.5) with a colorized elevation map and 100 m HRSC contours. The contour line that corresponds to the front of the Pancake delta is shown in white (−3280 m) to highlight where associated deposits to the west of the Pancake delta would have been deposited. The volumes of sediment associated with depositional features and the removed volumes of sediment from erosional features are also shown. The Pancake delta and its associated deposits (i.e., "incised plains"), the Farah Vallis fan-delta, and the Wall fan emanating from the upper half of Farah Vallis comprise 42 km^3 of material, which approximately matches the 40 km^3 of material removed to create Farah Vallis. Figure 5 shows a closeup view of the regions marked "Farah Vallis Upper and Farah Vallis Lower Incision," Figure 6 shows an up close view of the region marked "Farah Vallis delta," Figure 7 is a CTX image of the region marked "FV fan," and Figures 7 and 8 are a CTX image and contour map, respectively, of the region marked "Pancake delta."

On the southern rim of Gale crater the large v-shaped incised valley, recently named Farah Vallis (Figure 5), leads to Gale crater. The term "valley" is used rather than "channel" because the feature is much broader and deeper than the channel that cuts it. Farah Vallis is composed of two distinct canyons: one that crosses the rim and cuts into ejecta and one that cuts into deposits from the upslope canyon. In total, it is 82 km long, has an average slope of 6% (Figure 5), and varies in width from 500 m to 3 km. The upper portion of the canyon is incised 26 km back from the crater rim into Gale crater ejecta [see *Newsom et al.*, 2014, Figure 1] and terminates in an amphitheater-shaped headwall. There are just two, short, stubby tributary valleys. Although relatively sharp edged, the floor of Farah Vallis is covered with dunes and colluvium, in some areas with up to boulder-sized material (see HIRISE image ESP_018142_1735) indicating that it is partially infilled. The upper portion of the canyon has an average slope of 6%, calculated every 100 m using HRSC data but begins to steepen to 9% as the valley enters Gale crater. Here it is incising into a deposit located ~1000 m below the crater rim, perhaps formed from local slumping processes post-impact. Between 26 km and 46 km the canyon takes two 90° bends before terminating as the channel at the base of the canyon crosses the crater wall.

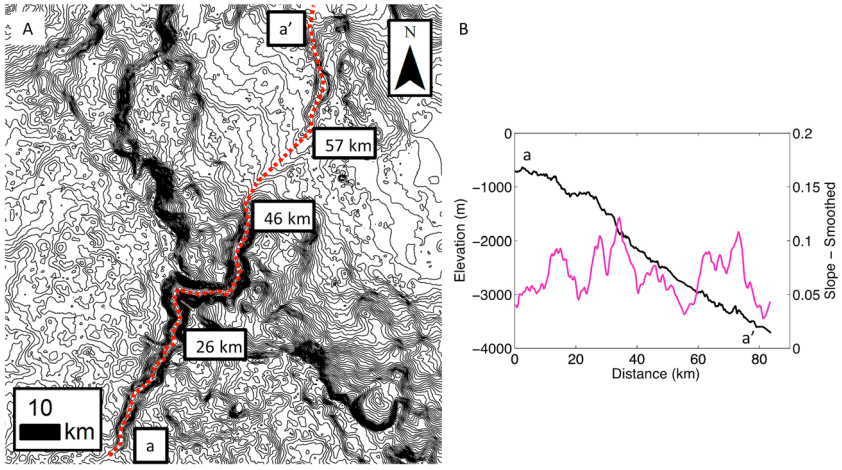

Figure 5. (a) 50 m HRSC contours for the Farah Vallis region are shown, as is the location of the longitudinal profile (a is upslope of a'). For perspective, the location of this region is highlighted in Figure S1. (b) A longitudinal profile (black line) and slope profile (pink line) of Farah Vallis. Elevation data were extracted from the HRSC DEM and plotted as a function of distance on the left *y* axis. Slope (pink line) was calculated every 100 m, and the 10 point average is plotted as a function of distance on the right *y* axis.

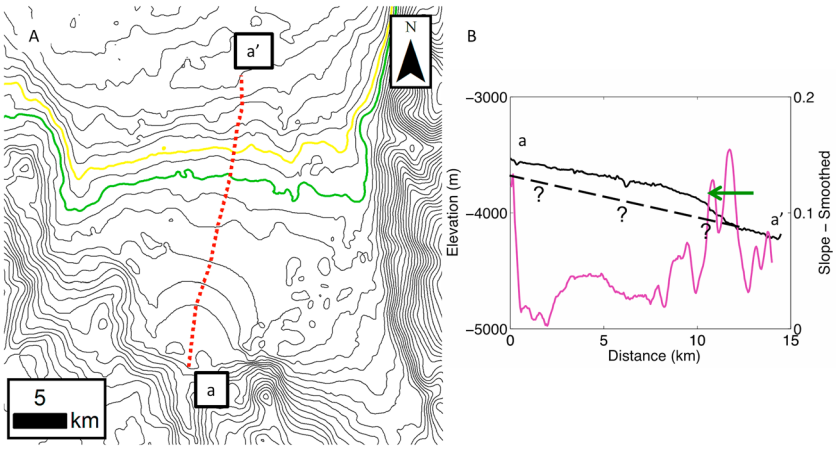

Figure 6. (a) 100 m HRSC contours of the Farah Vallis fan and delta are shown, as is the location of the longitudinal profile (a is upslope of a'). The location of the Farah Vallis delta is shown in Figure 4 as well as Figure S1. (b) A longitudinal profile (black line) and slope profile (pink line) of the Farah Vallis fan-delta. Elevation data were extracted from the HRSC DEM and plotted as a function of distance on the left *y* axis. Slope was calculated every 100 m, and the 10 point average is plotted as a function of distance on the right *y* axis. The −3780 m contour corresponding to the delta front is shown in green, with a green arrow pointing out the delta front within the longitudinal profile and slope data. For reference, the −3980 m contour is shown in yellow. A dashed line with question marks shows our topographic reconstruction of the crater floor.

Downstream of 46 km is a fan-shaped deposit (seen in CTX topographic data, Figure S2) with an average slope of 4%. We will refer to this as the Wall fan herein because of the location of the fan on the southern crater wall. Here Farah Vallis becomes less prominent, the valley width decreases from 1.5 km to 500 m and valley depth decreases from 200 m to 60 m in less than a kilometer and the channel crosses thick deposits (Figure 5). By about 57 km, the valley again incises, this time into prior deposits, with Farah Vallis widening again to a maximum of 2.5 km wide and 250 m deep before transitioning to a distinct fan-delta deposit (Figure 6).

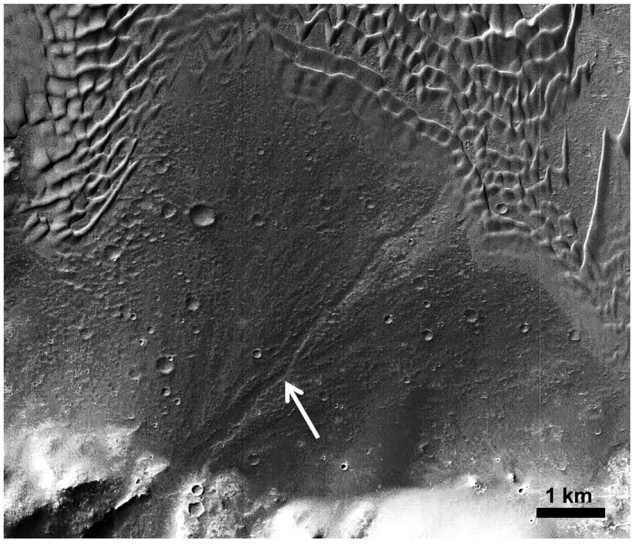

Figure 7. CTX image P13_006143_1745_XN_05S223W of the Farah Vallis (FV) fan deposit, whose location is indicated in Figure 4 (its arcuate convex contours can be seen in Figures 4 and 6), overlying the Farah Vallis delta deposit. This deposit covers approximately 25 km^2 and is relatively thin. It preserves a large channel running down its center that is nearly 5 km long.

At approximately the −3780 m HRSC contour (green contour, Figure 6a) there is an abrupt slope break from 5% to 12% (Figure 6b), which we infer to be the Farah Vallis delta front. The deltaic feature is 78 km^2 in planform area, has an average depth of 300 m, and a volume of 22.5 km^3. The volume is based on the analysis of 10 long profiles, and the assumption that the surface the delta aggraded across has the same slope as the regional surface slope for Gale crater (i.e., 1.4% sloping toward the north). The HRSC-derived contours (Figure 6) near the exit of Farah Vallis are strongly arcuate for the first 6 km, suggestive that there is an alluvial fan deposit overlying the Farah Vallis delta deposit. This overlying fan deposit (Figure 7) covers approximately 25 km^2 and is relatively thin, perhaps 15 to 20 m on average, based on extending the Farah Vallis delta surface back and underneath the hypothesized fan deposit. The fan deposit, referred to herein as the Farah Vallis fan,

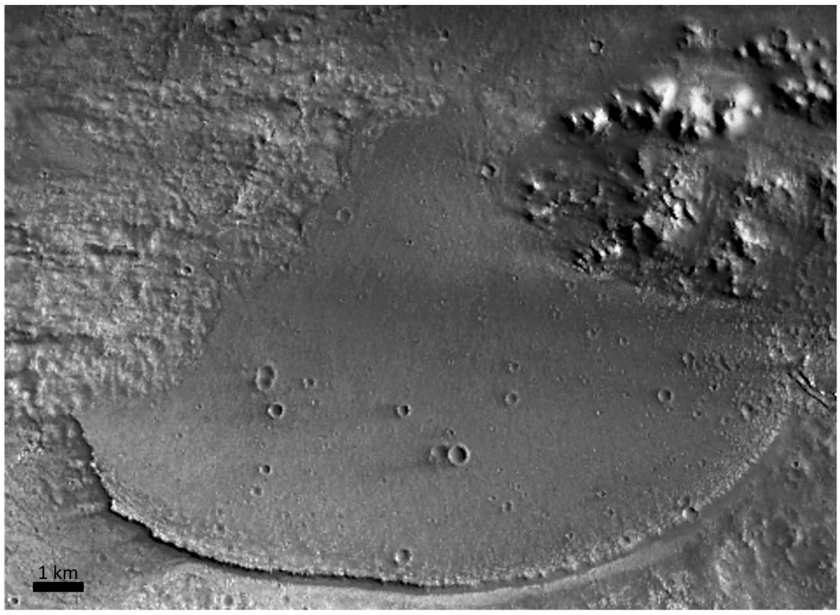

Figure 8. CTX image B21_017786_1746_XN_05S222W of the Pancake delta, which is a dark-toned, arcuate-shaped feature, which we interpret to be a classic Gilbert-type delta [*Gilbert*, 1890]. The location of the Pancake delta is marked in Figures 4 and S1.

while partially covered in dark sand from the nearby dunes, preserves a large channel running down its center (Figure 7). The channel is 5 km long, runs the entire length of the feature, and has a width of 80 m ± 10 m based on 20 measurements. HRSC data are too coarse to resolve channel depth.

To the east of Farah Vallis, and likely associated with erosion of Farah Vallis, is another depositional feature, which we infer to be a delta, referred to here as the Pancake delta (Figures 4 and 8). The Pancake delta is a dark-toned, arcuate-shaped feature that is 117 km^2 in planform and is approximately 100 m in depth. We estimate the deposit volume to be ~14 km^3 based on 10 long profiles. The delta has an average slope of 3% at its head, which decreases to 1.3% on its lower plain (Figure 9). At the delta front, which follows exactly the −3280 m HRSC contour line, the average slope increases abruptly to 13% (Figure 9b). There is only one HiRISE image of this delta (ESP_039491_1740), which covers the uppermost portion of the delta. The surface shows numerous nearly filled craters with rims mostly missing and no preserved channel-like features. The delta front, for which we only have CTX imagery (Figure 8), appears to be fairly well preserved. The front lacks any substantial gully development and maintains a relatively uniform height over 20 km.

The direct connection of Farah Vallis to the Wall fan, the Farah Vallis delta and fan, and its close association with the Pancake delta to the east, suggests that the sediment required to build these depositional features is derived from both the incision of Farah Vallis and from incision of sediment previously deposited from the Farah Vallis canyon. A quantitative test of this hypothesis is to compare estimates of the eroded and the depositional volumes (see Figure 4), as has been done by *Moore et al.* [2003] and *Howard et al.* [2005] in other environments.

Based on a combination of CTX and HRSC DEM data, the total eroded volume from Farah Vallis is 40.5 km^3 (Figure 4, 35.5 km^3 in the upper canyon, 5 km^3 lower incision). The Pancake delta and its associated deposits, which were later incised into, are 14 km^3 and 10 km^3 (5 km^3 was later eroded and deposited within the Farah Vallis delta), respectively. The Farah Vallis fan-delta deposit has a combined volume of 23 km^3, of which the fan is approximately 0.5 km^3. In total, the Pancake delta, Farah Vallis fan-delta, and the Wall fan emanating from the upper half of Farah Vallis comprise 42 km^3 of material, which approximately matches the 40 km^3 of material removed to create Farah Vallis.

3.2. The Entrance Canyon and Stacked Deposits

The Entrance Canyon ("EC" in Figure 3) is located on the north side of Mount Sharp (Figures 1 and 10) and is a destination for the *Curiosity* rover during its ascent of Mount Sharp. The large canyon within the lower Mount

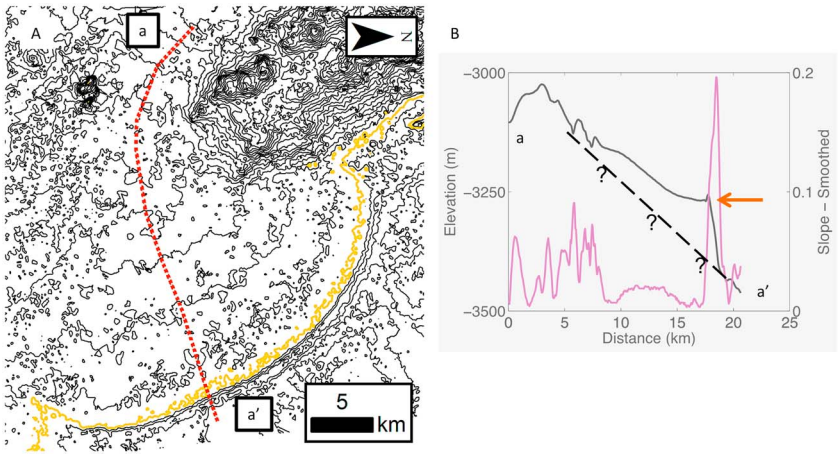

Figure 9. (a) 25 m CTX contours of the Pancake delta are shown, as is the location of the longitudinal profile (a is upslope of a'). (b) A longitudinal profile (black line) and slope profile (pink line) of the Pancake delta. Elevation data were extracted from the CTX DEM and plotted as a function of distance on the left *y* axis. Slope was calculated every 100 m, and the 10 point average is plotted as a function of distance on the right *y* axis. The −3280 m contour corresponding to the delta front is shown in orange, and an orange arrow points out the delta front within the longitudinal profile and slope data. Our topographic reconstruction of the crater floor is shown by a dashed line with question marks.

Sharp unit (referred to as the dark-toned layered yardang unit by *Anderson and Bell* [2010]) is ~4.5 km long. Upslope, the canyon appears to incise another ~6 km into the light-toned yardang unit [*Anderson and Bell*, 2010]. In the lower unit the canyon is on average ~850 m deep. Within this canyon there is an ~1 km long gully (colored in blue in Figure 11 and outlined in blue in Figure 12) with an average depth of 11 m and an average width of 150 m (based on 10 cross sections). The gully incised along an 11% slope. The gully is relatively sharp edged for most of its extent but is infilled with colluvium and meter-scale boulders (Figure 12b) and eventually transitions to a deposit first identified by *Anderson and Bell* [2010]. While they hypothesize that this deposit was once a large fan that has since eroded back, we propose here that it is actually a boulder-rich and crudely stratified series of deposits. Future rover observations, as discussed in section 7.2, can test these two hypotheses.

The uppermost deposit (numbered "1" and outlined in green in Figures 11 and 13) is relatively narrow with an average width of 140 m (five cross sections) and extends for ~750 m at an 8% slope (Figure 14). The depth ranges from 5 to 7 m. This upper deposit transitions to a second deposit (numbered "2" and outlined in red in Figures 11 and 13) that is wider, steeper sided and spreads radially. The front extends downslope for ~650 m and has an average slope of 12%, an average width of 270 (five cross sections), and an average depth of 32 m (this is inferred as we cannot follow this deposit all the way to the mouth of the gully). There is a clear front to this deposit (red arrow, Figure 13), which corresponds to the −3927 m HRSC contour, where it steepens from 12% to 40%. Based on the radial form and steep front, we interpret this deposit to be a delta. This deposit extends onto a second distinct deposit (numbered "3" and outlined in orange in Figures 11 and 13), which spreads laterally to the east and appears to have

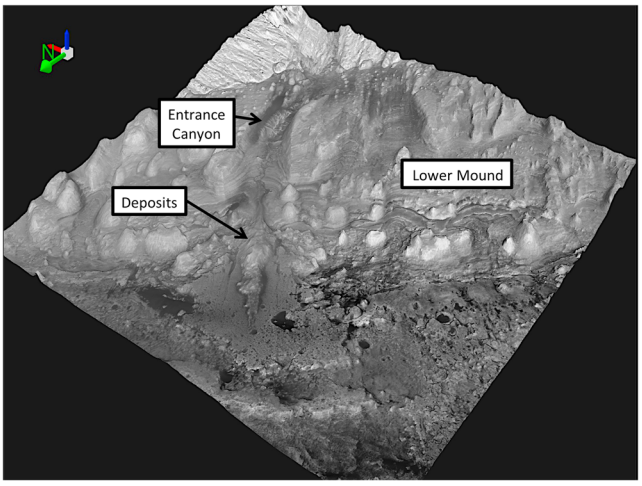

Figure 10. A close-up of the Entrance Canyon and its deposits (HIRISE image ESP_019698_1750 draped over the MSL-provided DEM [*Golombek et al.*, 2012]), as viewed looking southeast. For scale, the canyon is ~700 m wide near the arrow labeled "Entrance Canyon."

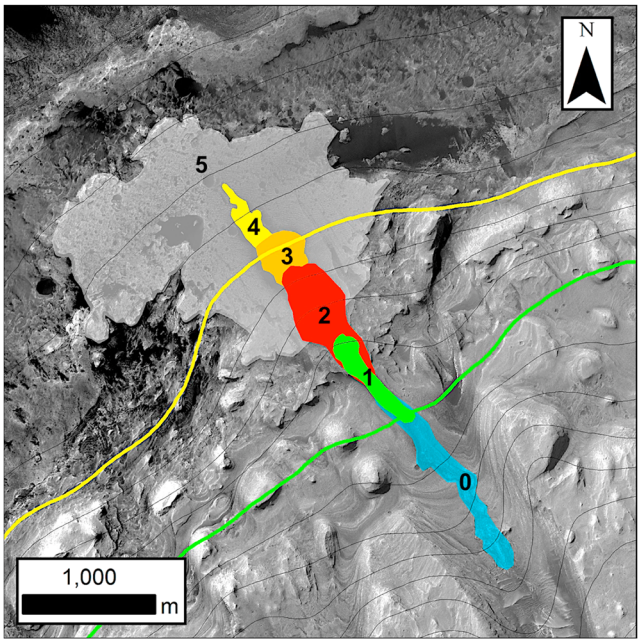

Figure 11. Within the Entrance Canyon there is an ~1 km long gully (0, blue) that eventually transitions to a boulder-rich, relatively narrow, and crudely stratified deposit (1, green). This upper deposit transitions to a second, likely deltaic, deposit (2, red) that is wider, steeper sided, and spreads radially. This deposit extends onto a second distinct deltaic deposit (3, orange), which spreads laterally to the east and appears to have inverted distributary channels. The lowest deposit is shown in yellow (4) and may preserve strata deposited by large-scale bedforms. Underlying the entire sequence is a broad, nearly uniform sloping plain (grey, 5). 50 m HRSC contours are shown, where the green contour represents the −3780 m HRSC contour (and corresponds very closely with the transition from the gully to the Entrance Canyon deposits) and the yellow contour represents the −3980 m HRSC contour. HIRISE image ESP_019698_1750.

inverted distributary channels. Again, based on its form and the presence of channels, we interpret this deposit to be a delta as well. This second delta front deposit extends ~260 m, is on average 255 m wide (10 cross sections), and ~11 m thick (this is inferred as we cannot follow this deposit all the way to the mouth of the gully). The delta front is located near the −3980 m HRSC contour line (yellow contour, Figure 11) and is characterized by a sudden change in slope from ~8% to 32% (orange arrow, Figure 14). The lowest deposit is shown in yellow in Figure 13 (and is numbered "4" in Figure 11) and extends another 520 m. This deposit has an average width of 160 m (10 cross sections) and is ~9 m deep where we can trace it out (we cannot follow this deposit all the way to the mouth of the gully). Underlying the entire sequence is a broad, nearly uniform sloping plain (colored in grey in Figure 11 and numbered "5"), with an average slope of 13% that is etched with strata that were deposited by well-defined, regularly spaced bedforms (spacing is approximately 20 m) with lighter-toned ridges oriented in an east-west direction (similar ridges were identified all around Gale and are discussed at length in *Milliken et al.* [2014]). No meter-scale material was observed in the HIRISE imagery on this plain, suggesting a fine grain size. However, based on examination of the HIRISE imagery, the sequence of deposits mapped in and overlaying this plain all appear coarse, containing meter-scale boulders, which is consistent with the steep slopes at which they deposited.

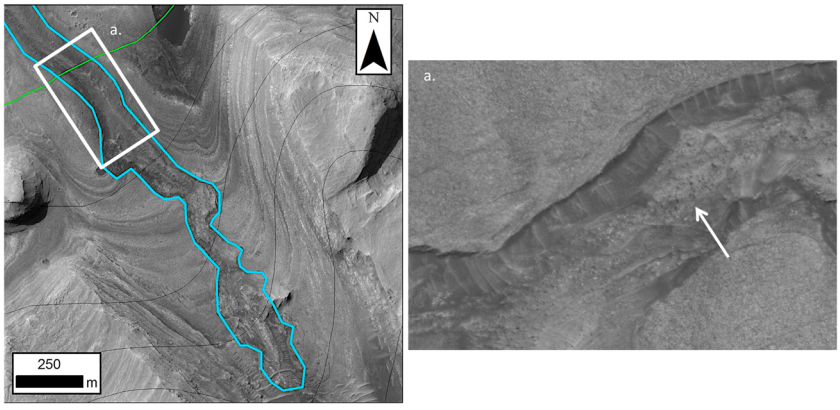

Figure 12. (a) A view of the gully (outlined in blue) within the Entrance Canyon with 50 m HRSC contours and (b) a closeup view of the region outlined in white (Figure 12a) showing the boulder-rich infill. HIRISE image ESP_019698_1750.

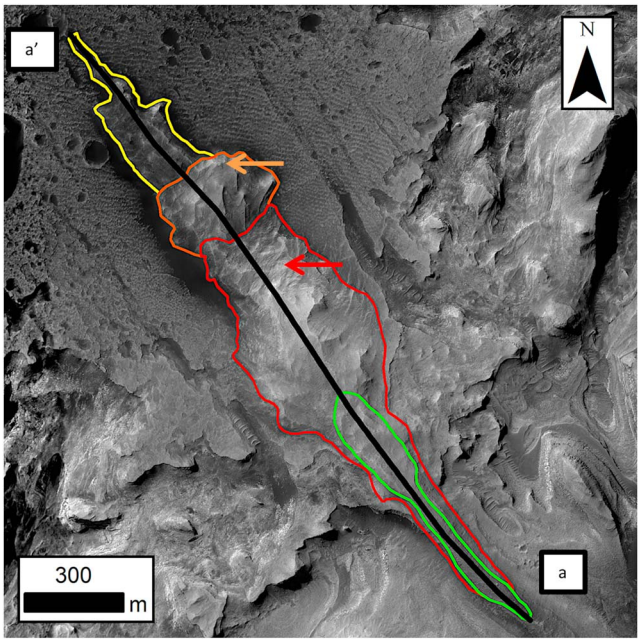

Figure 13. A similar view as shown in Figure 11 except that the Entrance Canyon deposits are outlined to better show their morphology and texture. The location of the longitudinal profile in Figure 14 is also shown (black line, a is upslope of a'; HIRISE image ESP_019698_1750).

Combined, the coarse, steep nature of the deposits and the break in slope like that of a delta for at least two of the deposits, argues for distinct onlapping stratigraphy. Figure 15a shows the transition from deposit 2 to deposit 3, and Figure 15b shows the transition from deposit 3 to deposit 4. In both cases, there are distinct changes in texture, brightness, layering, and the presence or lack of ridges (inferred to be paleochannels), suggestive that these deposits were deposited in different events and likely were sourced from different upslope materials. The stacked, stair-stepping character of this delta is consistent with a feature formed during a time of water level rise, where the stepped topography is caused by the lateral migration of delta front lobes that shift landward as water levels rise but are unable to cover lobes of older cycles [e.g., *Muto and Steel*, 2001].

Using 1 m HIRISE elevation data, the volumes of each deposit were calculated using both long profiles and cross sections and were compared to the removed gully volume of 0.004 km^3. We calculated the gully volume using its length, average width, and depth. As a portion of the gully is currently backfilled (Figure S3), we had to project the gully floor surface under these deposits to get an estimate of the pre-backfilled gully depth and hence the pre-backfilled gully volume. We estimate that the uppermost deposit (1, green, Figure 11) is ~0.0007 km^3, the first underlying delta deposit (2, red, Figure 11) is ~0.01 km^3, the second delta deposit (3, orange, Figure 11) is ~0.005 km^3, and the lowest deposit (4, yellow, Figure 11) is ~0.003 km^3. In total, the entrance canyon deposits are estimated to be ~0.018 km^3 in volume, which is ~5 times larger than the volume of material excavated from the gully. While these volume estimates will be refined as *Curiosity* gets closer to these deposits and the stratigraphy can be more carefully mapped via Mastcam imagery, the general result (i.e., the gully is undersized compared to the deposits) is unlikely to change. This suggests, perhaps, that the feeder gully was once larger in extent or depth and has mostly been filled in since it was last active. Evidence for the latter is the presence of large boulders, colluvium, and modern aeolian dunes that are obscuring the head of the gully (Figure S2). The gully may have not been the only sediment source for these deposits, as there is very coarse debris lying in the well-defined canyon upslope and dark scree and colluvium lying at the base of the east facing cliff, both of which would be a ready source of debris for runoff from Mount Sharp.

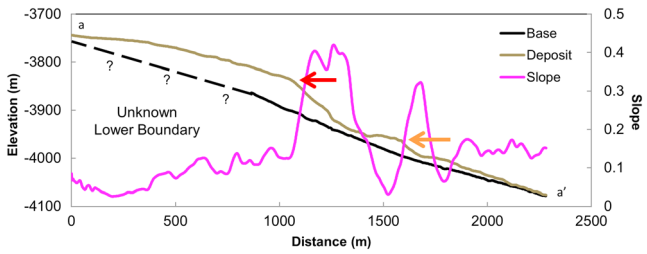

Figure 14. A longitudinal profile (brown line) and slope profile (pink line) of the Entrance Canyon deposits, as well as the long profile of the surface (black line) upon which the deposits lie. Elevation data were extracted from the HIRISE DEM and plotted as a function of distance on the left *y* axis. Slope was calculated every 10 m, and the 10 point average is plotted as a function of distance on the right *y* axis. A red arrow is pointing out the −3980 m delta front, and the orange arrow is pointing to a second possible delta front.

3.3. The Dulce Vallis Delta System

On the northwestern rim of Gale crater is a third delta system (Figures 1 and S4), referred to here as the Dulce delta (as it emanates from Dulce Vallis), though there are actually three distinct inferred

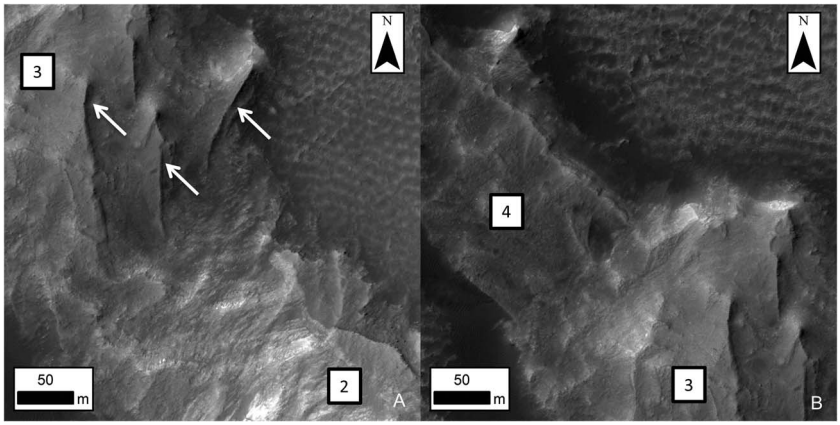

Figure 15. (a) Deposit 2 appears to be a distinct deposit onlapping deposit 3, which has thin ridges perpendicular to contour and spreading out radially (white arrows), suggestive that these are recording past channels that are now inverted. (b) Deposit 3 appears to be onlapping deposit 4. HIRISE image ESP_019698_1750.

delta deposits. The lower more prominent deposit ("DD1" in Figure 3) has a front that corresponds to the −3980 m HRSC contour (yellow contour, Figure 16a). As seen with previous deposits, the slope rapidly increases downslope at this front, in this case increasing from an average slope of 13% to 21% (Figure 16b). This deposit is approximately 7.0 km^2 in planform and is 250 m thick at its front. A second, smaller delta deposit (DD2) is overlaying it in a stair-step morphology [*Muto and Steel*, 2001; *Kraal et al.*, 2008], and its front corresponds to the −3780 m HRSC contour (green contour, Figure 16a). Again, there is an abrupt increase in slope from 7% to 14% (Figure 16b). The deposit has a planform area of 2 km^2 and is 100 m deep at its front. To the south is a second, smaller deposit (DD3) whose front also corresponds to the −3780 m HRSC contour (green contour, Figure 16a). This deposit has an area of 0.3 km^2 and is 50 m deep at its front. Directly to the north of these delta deposits is perhaps a small fan, based on its form and convex contours (Figure 16a, black arrow). This small fan feature has an area of 6 km^2 and a slope of 12%. Based on CTX imagery, the deltaic deposits are all light toned, appear to be minimally eroded into at their fronts (there is no gullying or evidence of wave cutting at the scale of the imagery), and there are no observable channel-like features.

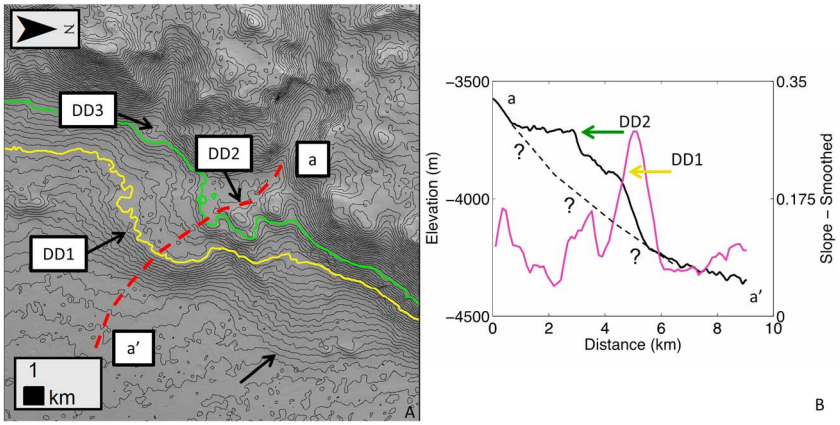

Figure 16. (a) 25 m CTX contours of the Dulce Vallis system (the green contour is the −3780 m HRSC contour, and the yellow contour is the −3980 m HRSC contour), highlighting the location of the Dulce Vallis deposits (DD1, DD2, and DD3) and the small fan (black arrow); the location of the longitudinal profile in Figure 16b is marked with a red dashed line (a is upslope of a'). (b) A longitudinal profile (black line) and slope profile (pink line) of the Dulce Vallis deposits. Elevation data were extracted from the CTX DEM and plotted as a function of distance on the left *y* axis. Slope was calculated every 100 m, and the 10 point average is plotted as a function of distance on the right *y* axis. A yellow arrow is pointing out the −3980 m delta front, and a green arrow is pointing out the −3780 m delta front within the longitudinal profile and slope data. A dashed line with question marks shows our topographic reconstruction of the crater wall upon which the deposit lies.

Upslope of the Dulce delta and fan deposits is a branched valley network, Dulce Vallis. The valley network is 76 km long, has an average slope of 8% (Figure S5), and varies in width from 250 m to 1.6 km. Using the current surface topography from both HRSC and CTX to infer the direction of transport of water and sediment, a watershed area of about 450 km^2 drains to the Dulce delta system. The drainage density for Dulce Vallis is 0.16 km/km^2. This is higher than some of the highest valley network drainage densities reported in a global survey by *Hynek et al*. [2010] of over 82,219 valleys and in the same range of values as the dense valley networks studied in Noachian terrains at a similar scale in HRSC DEMs [*Ansan and Mangold*, 2013]. The source area farthest back from the crater rim consists of gently sloping plains toward Gale crater (5% slope on average) interspersed with local mounds and ridges, perhaps formed from impact ejecta, which are roughly 50 to 100 m in relief. There are local bedrock exposures, but only at the steepest portions of the hills, as most of these mounds and ridges are mantled with debris, likely colluvium or aeolian deposits. The overall appearance of the Dulce Vallis watershed is one of disrupted topography associated with impacts and impact ejecta that has been mantled by outfall from airborne sediment, colluvium from retreating slopes, and possibly fluvial reworking. The valley system, with limited amphitheater-shaped headwalls, drains to the Dulce delta and is cut into the previously deposited sediments. Although relatively sharp edged, the incised valleys are also floored with dunes and colluvium, indicating that they are partially infilled.

Using 18 m CTX DEM data, the total volume of material that has been eroded from the Dulce Vallis network is 1.6 km^3. Both methodologies for calculating the volume of the deltaic deposits were performed for the Dulce delta deposits (i.e., topographic reconstruction of the pre-delta crater floor and long profile analysis) resulting in an average net deposit volume of 1.5 km^3. We do not have a strong constraint on the volume of the small fan, but by projecting the local topographic slope of the crater floor underneath the fan deposit, its average depth is approximately 15 m. A planform area of 6 km^2 gives an approximate volume of 0.09 km^3. The sum of the two prominent delta volumes and the small fan is 1.59 km^3, which is an approximate balance between the volumes of material eroded in forming the valley network (1.6 km^3). Assuming that the delta deposits have not been substantially eroded (as suggested by the close sediment balance between erosion and deposition), the stacked morphology of DD2 on DD1 suggests that like the Entrance Canyon deposits, Dulce valley deltas may record a period of lake level rise.

3.4. Peace Vallis and Fan System

Palucis et al. [2014] provide a detailed description of the Peace Vallis fan system (Figure 1), so just a brief overview is provided here. The lower, fine-grained deposits of the Peace Vallis fan were extensively explored by the Curiosity rover and, consistent with expectations from the geomorphic setting, lacustrine deposits were identified [*Grotzinger et al*., 2014; *Vasavada et al*., 2014]. The Peace Vallis fan is defined by convex contours that extend across the lower portion of the northern Gale crater wall [*Palucis et al*., 2014, Figure 5]. The fan is a single geomorphic unit that covers about 80 km^2 and is laced on its western margin with frequent ridges interpreted to be paleochannel beds [*Palucis et al*., 2014, Figure 5]. The fan's apex is located at the −4227 m HRSC contour, which is 150 m lower than the lowest Dulce delta front (DD1) and 100 m lower than the bottom of the platform associated with the Entrance Canyon deposits. It is topographically one of the lowest hydrogeomorphic features in Gale crater (Figure 3).

The location of the Peace Vallis fan likely results from a 15 km setback in the crater rim (Figure 12a) [*Palucis et al*., 2014], which enables drainage from the adjacent plains near the crater rim to spill into a canyon where an incised valley feeds the apex of the fan. This incised valley network, which is 107 km long, was fed by a catchment area 730 km^2 in size, resulting in a drainage density of 0.15 km/km^2. Similar to Dulce Vallis, all of Peace Vallis appears to be excavated into previously deposited debris. Estimates of volume removed to form the incised valley (0.8 km^3) match the total volume of the original, pre-eroded fan (0.9 km^3).

3.5. South Fan System

There is a large fan deposit, referred to here as the South fan, off of the southern rim of Gale (Figure 1). The fan covers an area of 240 km^2 with an average slope of 1.5%. The fan apex is located 200 m above the −3280 m HRSC contour line, and its distal end is approximately 100 m lower. CTX imagery did not reveal any shorelines or gullying into the fan deposit at −3280 m, though it is very possible that these features would not be resolvable at this scale (6 m/pixel). A dark dune field covers the upper portion of the fan, but the lower portion of

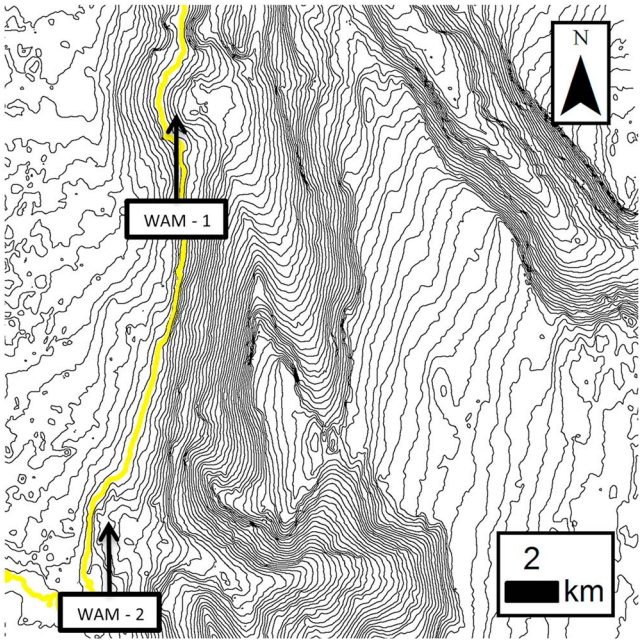

Figure 17. Along the western margin of Mount Sharp, small ($< 3\ km^2$) complex fan-delta-shaped deposits lie at the mouth of two of the larger canyons that exit to the Gale floor. These deposits may be small deltas recording fluvial activity in the upslope canyons, but there is only a minor amount of sediment delivery relative to the scale of the canyons. The −3980 m HRSC contour (Dulce Vallis lake stand, yellow) that defines the lower Dulce Delta (DD1) crosses both these small deltas at approximately the elevation where downslope steepening occurs.

the fan is light toned, preserves some small channel features, and has a pitted appearance, likely from impact cratering. The low resolution HRSC DEM precludes an accurate volume estimate of this relatively thin feature.

3.6. Small Fans, Small Deltas, and Channels Around Gale Crater

Along the crater walls and from the slopes of Mount Sharp are gullies, sinuous ridges (likely inverted channels), and small deposits that based on their form and location also likely record deltas and fans. Previous maps have been published that capture many of these features [e.g., *Anderson and Bell*, 2010; *Le Deit et al*., 2013; *Milliken et al*., 2014]. Here we focus on attributes of those features that may provide clues about lake levels and their relative timing.

To the east of the Farah Vallis delta-fan system is a small delta-like feature emanating from a large canyon on the south side of Mount Sharp (Figure S6). *Milliken et al*. [2014] also identified fan-like deposits emanating from the canyons to the east of our delta-like feature ("fan 1" and "fan 2" in their Figure A4) that are underlain with preserved bedforms similar to those under the Entrance Canyon deposits. The apparent front of this small delta roughly corresponds to the −3280 m HRSC contour line, though the HRSC DEM is too coarse to get a longitudinal profile to assess if there is an obvious break in slope (and thus define the shoreline boundary). The feature is approximately 0.5 km^2 in area and thinner than that which can be documented using 50 m HRSC contour intervals. Based on CTX imagery, the delta-like feature does show what may be inverted distributary channels, indicating that erosion of the deposit has occurred since deposition. The canyon immediately upslope from the feature has an average depth of 150 m and an average width of 1.7 km. Since the feature is obviously underscale relative to the canyon from which it emerged, it likely records only a small portion of the sediment derived in cutting the upslope canyon. There is also a close correspondence of the termination positions of inverted channels (as mapped by *Anderson and Bell* [2010]) and the −3280 m HRSC contour (i.e., the Pancake lake stand) (Figure S7). This suggests that while flow and sediment from Mount Sharp may have been channelized across fans (like those shown in *Milliken et al*. [2014]), when these channels reached standing water, they dispersed and deposited their sediment load. Where we see inverted channels today might be due to former channel beds providing protective gravel armor from wind erosion [*Williams et al*., 2009].

Along the western margin of Mount Sharp, small ($<3\ km^2$) complex fan-delta-shaped deposits (named the Western Aeolis Mons (WAM) deposits—see Figure 3) lie at the mouth of two of the larger canyons that exit to the Gale floor (Figure 17). These roughly arcuate-shaped deposits are strongly wind scoured, and this deflation in the more southern deposit (WAM-2) has exposed subtle crossing ridges that may record channels. There is an elevation difference of 500 m from the top to the bottom of the larger deposit (WAM-1) and a 250 m difference for the smaller deposit (WAM-2) with slopes of 20% to 27%. Collectively, these attributes suggest that both deposits record small deltas driven by fluvial activity in the upslope canyons but minor amounts of sediment delivery relative to the canyon scales. The −3980 m HRSC contour (yellow) crosses both these small deltas at approximately the elevation where downslope steepening occurs (Figure 17). This elevation corresponds to the DD1 delta front and the Entrance Canyon deposit 3 (Figure 3).

In general, small fan development along the crater walls of Gale is concentrated on the northeast wall (Figure 1). These fans were first mapped and discussed in *Anderson and Bell* [2010]. The fans are typically 1 to 40 km^2 in area and deposit on slopes between 8% and 16% (using CTX slope data). In appearance, the fans are thin, appear to preserve craters thus giving them a pitted texture, and often have ridges, inferred to be paleochannels by *Anderson and Bell* [2010], running perpendicular to contour. These somewhat sinuous ridges often continue past where the fan form ends, sometimes continuing to the crater floor.

Incised channels are most numerous along the northeastern wall where the crater rim is least sharply defined (Figure 1). Larger and deeper incised channels are developed along the southern wall. Most of the incised channels do not terminate in fans, suggesting that there is a threshold volume of erosion for a fan to be supported and/or preserved, which we calculate to be ~0.5 km^3. In the southern half of Gale, the incised channels show no correspondence to proposed lake levels (three colored contours in Figure 1). In the northern half of Gale, however, there appears to be a correspondence between the termination point of channels cut into the crater wall and the level of the two proposed lake levels (−3780 and −3980 m HRSC contour lines). Approximately, half terminate at the −3780 m level and half terminate at the −3980 m level, suggesting a possible coincidence in channel incision and lake level timing.

4. Identification and Sequencing of Three Major Lake Stands in Gale Crater After Mount Sharp's Formation

Based on the geomorphic evidence presented above, we hypothesize that there were at least three major lake stands within Gale crater, post-Mount Sharp, that endured long enough to leave a geomorphic record (i.e., a deltaic deposit) of their existence (Table S2 and Figure 3). Each of these lake stands will be described and then a possible sequence of lake level decline followed by lake level rise is proposed.

4.1. Pancake Lake Stand (−3280 m HRSC Lake Level)

Within Gale crater, we interpret the highest lake level (based on the deposits described in section 3) to have reached about the −3280 m HRSC contour (orange contour in Figure 1, orange star in Figure 3) and is defined most clearly by the Pancake delta, though the small delta off of Mount Sharp also terminates at this elevation. In addition to these delta features, this elevation also corresponds to the termination of several small inverted channels off of the southern flank of Mount Sharp (Figure S7). A lake at this elevation would have covered a surface area of 5832 km^2 and would have had a mean depth of 0.7 km. This lake would have occupied a volume of 3780 km^3. This assumes that Mount Sharp was at its current extent and that relatively little erosion and/or infilling of the crater floor has occurred since the time of these lakes.

4.2. Farah Vallis Lake Stand (−3780 m HRSC Lake Level)

The second highest lake level is at the −3780 m HRSC contour (green contour in Figure 1 and green star in Figure 3) and is defined most clearly by the Farah Vallis delta front and also corresponds to the upper Dulce delta (DD2) and the termination of approximately half of the gullies on the northern wall of Gale crater. It is also near the elevation where the gully within the Entrance Canyon transitions to a deposit. A lake at this elevation would have covered a surface area of 3617 km^2 and would have had a mean depth of 0.4 km. The lake would have occupied a volume of 1583 km^3.

4.3. Dulce Vallis Lake Stand (−3980 m HRSC Lake Level)

The third highest lake level would have occurred around the −3980 m HRSC contour (yellow contour in Figure 1 and yellow star in Figure 3) and is defined most clearly by the lower Dulce delta (DD1, Figure 16) and the middle delta within the Entrance Canyon deposits (deposit 3 outlined in orange, Figure 11). This elevation also corresponds to the termination of the other half of the gullies on the northern wall of Gale crater. A lake at this elevation would have covered a surface area of 3008 km^2 and would have had a mean depth of 0.3 km. The lake would have occupied a volume of 915 km^3.

4.4. Proposed Sequence of Lake Levels

An important interpretation of our analysis is that all the channel and depositional features we have mapped postdate the evolution of Mount Sharp close to its present form. The evidence for this seems substantial. The correspondence between erosion and deposition in the Farah Vallis, Dulce Vallis, and Peace Vallis systems and the relatively sharply preserved erosional and depositional forms makes it unlikely that these features

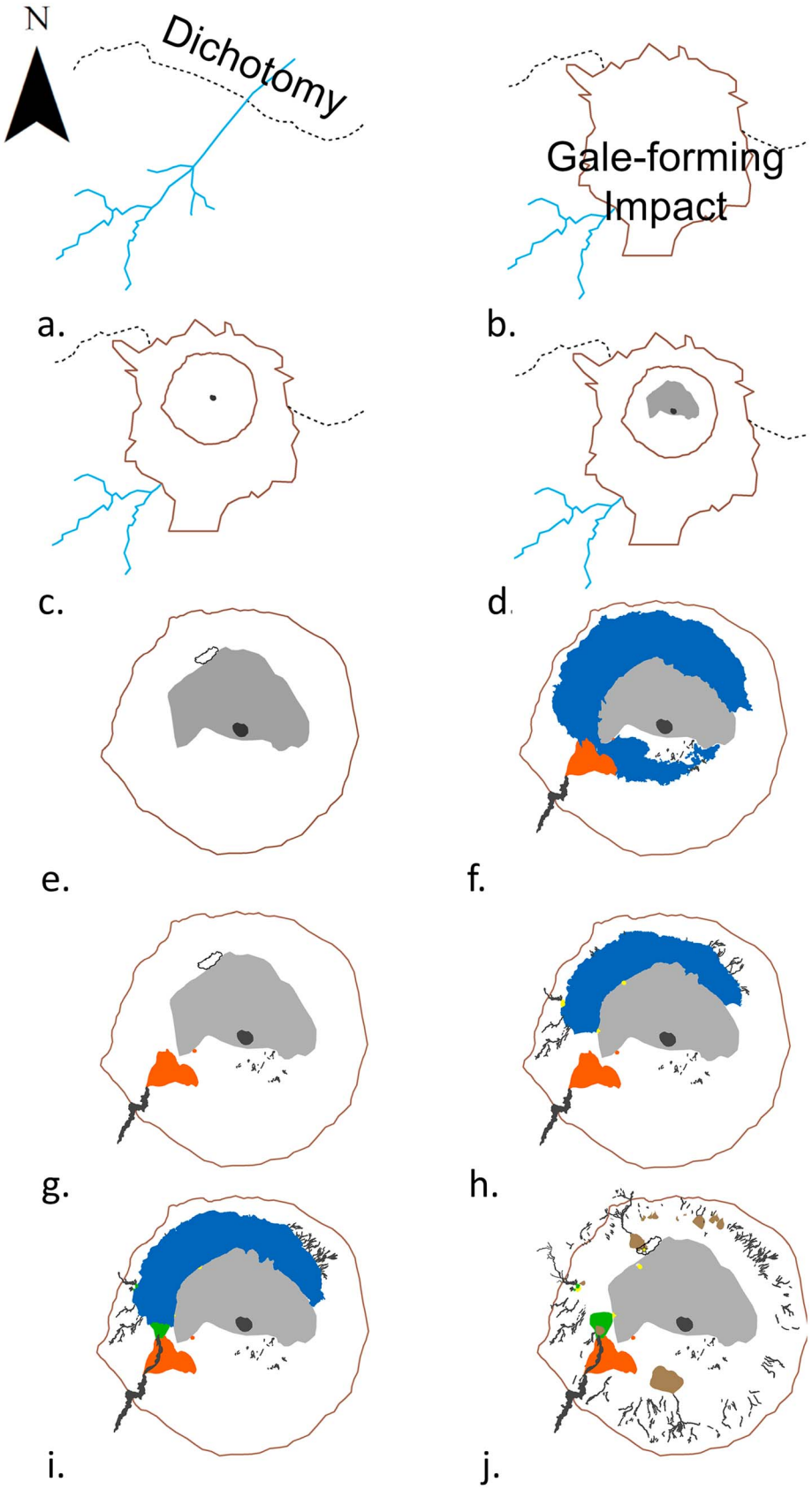

Figure 18

were once buried under a more laterally extensive central peak deposit and then exhumed to the present state. Of course, since deposition of these features, some erosion/deflation has likely occurred based on the presence of inverted features on, for example, the Peace Vallis fan. All of the erosional and depositional features mapped on Mount Sharp appear to be related to the current Mount Sharp topography (channels associated with definable upslope valleys), and the correspondence of elevations of features on the crater walls and Mount Sharp further argues for them to have formed after Mount Sharp reached close to its present topographic state.

There was likely a preexisting channel network across the landscape struck by the Gale impact (Figure 18a), but the subsequent ejecta blanket that surrounds Gale was not deeply incised by that system [*Irwin et al*., 2005]. Nonetheless, the approximately 290,000 km^2 watershed that drained across the pre-Gale landscape may still have received water via subsurface and surface flow from this directed watershed and the water entering Gale crater then could contribute to the incision of Farah Vallis [*Irwin et al*., 2005]. This does imply a delay in that incision until Aeolis Mons had developed and the floor of Gale crater reached approximately its current topographic form (Figures 18b–18f).

A key to understanding the subsequent sequencing of lake levels within Gale once Mount Sharp had developed is the pattern of dissection of the Wall fan emanating from Farah Vallis. After Aeolis Mons reached close to its current topographic form, water supplied from the south breached Gale crater and began to incise Farah Vallis and deposit sediment. Once the lake level rose to the Pancake lake stand (−3280 m), sediment would have initially deposited within the Pancake delta, before spilling toward the north (region mapped in orange in Figure 19). The lake level likely never rose above the Pancake delta, as the Wall fan that appears to have formed during the time of the Pancake delta and its associated deposits (region mapped in red in Figure 19) maintains a relatively constant slope of 4% and does not show any topographic indications at the resolution of CTX DEM data that its distal end formed subaqueously (e.g., rapidly decreasing slopes or decreasing convexity of contours, Figure 9). The switch from delta formation to fan formation on the crater wall was likely the result of decreased runoff (and hence reduced transport capacity), decreases in sediment supply [*Stock*, 2013], or simply the spreading of unconfined flow from Farah Vallis toward the northwest. In all cases, the end result was significant, sediment was not delivered to the Pancake lake stand level, and hence, no delta formed to the west of the Pancake delta. As water and sediment were being delivered to build the Wall fan it is clear that runoff did not outpace evaporative losses and the Pancake lake high stand declined. Evidence for this decline is the later incision into the Wall fan combined with the lower elevation (−3780 m) Farah Vallis delta front. Based on our mass balance analysis, incision into the Wall fan, either from runoff or groundwater seepage, eventually supplied the remaining sediment needed to build the Farah Vallis fan-delta complex (region mapped in green and brown in Figure 19).

After the Pancake delta lake stand, water levels must have dropped. As to how low it dropped, if the Entrance canyon and Dulce delta deposits record a backstepping sequence (i.e., rising lake levels, as was proposed in sections 3.2 and 3.3), then after the Pancake delta lake stand, water levels must have at least dropped below the Entrance canyon deposits (Figure 18g). The lowest deposit from the Entrance canyon terminates near the

Figure 18. A cartoon representation of a plausible hydrologic sequence within Gale crater since its impact: (a) development of an incised valley network that drained the Noachian terrain near Hershel crater. (b) Gale's crater-forming impact occurred during the late Noachain/Early Hesperian. (c) Gale crater's ejecta blanket (outer brown line) disrupted the valley network to its south; prior to Aeolis Mons development; Gale likely had a central peak (black dot) (d) growth of Aeolis Mons (grey), perhaps due to infilling and subsequent excavation of Gale crater [*Malin and Edgett*, 2000] or from slope-enhanced aeolian transport and deposition [*Kite et al*., 2013]. (e) Perhaps coeval with Aeolis Mons's growth is the deposition of sediment from the northern crater rim to Gale, forming the 15 km setback in the rim into which Peace Vallis eventually formed (and may have resulted in the complex topographic boundary conditions that the Peace Vallis fan encountered at its distal end, including a 64 km^2 basin shown by the black contour [*Palucis et al*., 2014]). (f) Incision of Farah Vallis due to renewed runoff from the south and the subsequent deposition of the Pancake delta and the plains to its west, which record one of the largest lake stands to have occupied Gale (−3280 m HRSC contour). (g) Decreasing runoff resulted in the decline of the −3280 m lake stand, perhaps completely but at least to a level lower than the entrance canyon deposits. (h) Local precipitation that drove incision of the crater rim and Aeolis Mons (and perhaps some renewed runoff from Farah Vallis) leads to a second high stand in Gale at −3980 m. (i) Further runoff, as evidenced by the incision of more gullies around Gale's rim and the formation of the Farah Vallis delta front (requiring incision into the wall fan and plains to the west of the Pancake delta), leads to the second highest stand in Gale at −3780 m. (j) The −3780 m lake stand rapidly declines and disappears, based on the lack of gullying of the lower delta deposits, leading to a period of fan (and gully) formation around Gale.

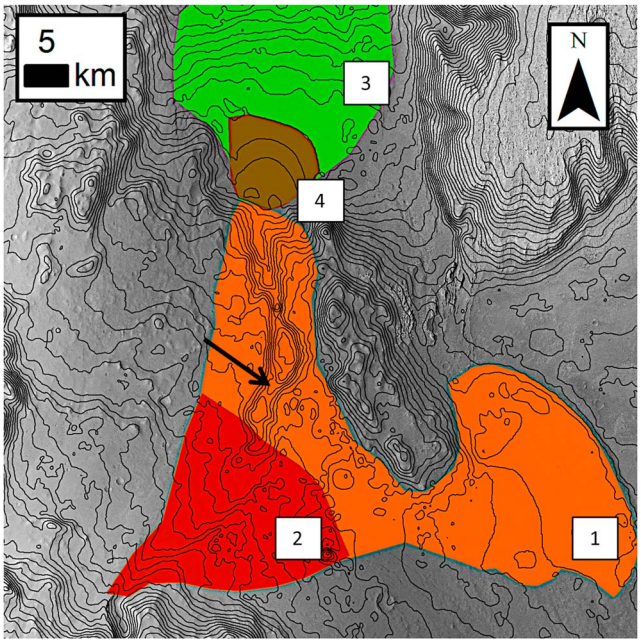

Figure 19. An overview of the lower Farah Vallis region, in which the four main deposits have been mapped. Initial incision of Farah Vallis leads to the Pancake delta and its associated deposits to the west (1, orange), followed by deposition of the Wall fan (2, red). Later incision into the "Pancake delta associated deposits" and the Wall fan (black arrow) resulted in the deposition of the Farah Vallis delta (3, green) and Farah Vallis fan (4, brown). As it incises into the Wall fan (2), Farah Vallis becomes less prominent, decreasing in valley width and depth, but at its lower end, Farah Vallis widens again before transitioning to the Farah Vallis fan-delta deposit.

−4077 m HRSC contour, suggesting that the lake would have dropped to at least this level. This corresponds to an 800 m elevation drop and losses of 1034 km^3 of water. We have not observed shorelines or strandlines around Gale crater that definitively point to a lake below or near the elevation of the Entrance canyon platform, though pressure and wind conditions on post-Noachian Mars may have constrained wave and shoreline development [*Banfield et al*., 2015] or it was a short-lived period of standing water. The lake may have also disappeared entirely; this lacustrine hiatus between the Pancake and Dulce Vallis lake stands (Figure 18g) could have lasted for a long time.

The common elevation of the steep front of the middle Entrance canyon deposit (deposit outlined in orange, Figures 11 and 13) with the steep front of the lower Dulce delta (DD1, yellow contour, Figure 16), suggests that at some point the lake rose to approximately −3980 m (Dulce Vallis lake stand) and remained there long enough to build these deposits (Figure 18h).

Several observations suggest that the lake level rose again from the −3980 m Dulce Vallis lake stand to the −3780 m Farah Vallis lake stand (Figure 18i). Our mass balance analysis suggests that deltas DD1 and DD2 are minimally eroded, so it is unlikely that the stacked form is somehow the result of wind erosion. Hence, we interpret the stair-stepped morphology observed as recording an increase in lake level resulting in a level that persisted long enough to build the upper Dulce delta deposit (DD2) atop the lower Dulce delta deposit (DD1) (as discussed in section 3.3). Similarly, we observe what appears to be a backstepping sequence at the Entrance canyon deposits (as discussed in section 3.2). We cannot close the sediment budget here, but the steep slopes of these deposits (Figure 18b) combined with the observation that they are composed of coarse-grained boulder-rich material suggest that these deposits are also likely to be minimally eroded and are therefore recording lake level rise. We do not observe boulders being planed off and covered with saltating sand as was observed by *Golombek et al*. [2014] on Meridiani Planum as we might expect if these boulder deposits were being wind eroded, but this also may not be visible in HiRISE imagery. In either case, we do not observe cuts or gullying into the upper delta deposits, as one might expect if these deposits were the result of falling lake levels. Lastly, we do not see incision into the Farah Vallis delta deposit or the DD2 and DD3 delta deposits, which we would expect to see if lake levels had decreased from the Farah Vallis stand to the Dulce Vallis lake stand. It is during this lake stand that the majority of the incision into the Wall fan and plains to the west of the Pancake delta occurred, as this incision supplied the sediment needed to build the Farah Vallis fan-delta complex (Figure 19).

The presence of a small fan atop the Farah Vallis delta suggests, perhaps, that following the last-detected lake stand (i.e., the Farah Vallis lake stand), a sudden reduction in flow from Farah Vallis led to rapid lake level decline and a period of fan building (Figure 18j). The large South fan, the smaller fans deposited on the northern rim of Gale, and the Peace Vallis fan may have then been the last major hydrogeomorphic events within the crater.

The Peace Vallis Fan is the most important, as it was located within the MSL landing ellipse, and its distal sediments were studied by the Curiosity rover [e.g., *Grotzinger et al*., 2014; *Vasavada et al*., 2014]. The Peace Vallis fan's apex is located at the −4227 m HRSC contour, making it one of the topographically lowest hydrologic features in Gale Crater (Figure 3). If the fan had been deposited prior to the large lakes, then one might expect to find much poorer topographic preservation. As this is not observed in the HiRISE imagery (0.25 m/pixel), it is likely that the Peace Vallis fan, similar to the Farah Vallis fan, occurred after lake level decline.

5. Hydrologic Conditions Driving Lake Dynamics

These documented lake stands imply a period of steady state lake level, which provides an opportunity to estimate the rate of water influx into the crater. We use these steady state discharges, combined with estimates of how much runoff is needed to build a depositional feature, to evaluate how long these lakes may have persisted. Theoretical and experimental estimates of evaporation rates on present-day Mars typically vary from 0.03 to 0.4 mm/h but could perhaps be as high as 2.5 mm/h [*Ingersoll*, 1970; *Hecht*, 2002; *Kuznetz and Gan*, 2002; *Sears and Chittenden*, 2005; *Sears and Moore*, 2005], though the lack of constraints on the temperature and pressure conditions of early Mars makes these estimates highly uncertain. While evaporation rates do increase with decreasing pressure, they are even more strongly a function of temperature, so that water at 0°C on present-day Mars will evaporate no faster than water at 60°C on Earth [*Hecht*, 2002]. A warm, wet early Mars [*Craddock and Howard*, 2002], therefore, may not have had orders of magnitude differences in evaporation rates as a cold, dry early Mars [*Head and Pratt*, 2001]. In lieu of better estimates at this time, we will use this range of values (0.03 to 0.4 mm/h) for the three hypothesized lake stands in Gale crater. At the highest stand, this equates to a steady state discharge, calculated as the product of lake area and evaporation rate, between 49 and 650 m^3/s (or 1.5 to 20 km^3/Earth year). *Wallace and Sagan* [1979] showed that for a range of Martian insolations, wind regimes, and pressures, the mean evaporation rates for ice-covered water bodies between 210 and 235 K is 10^{-8} g/cm^2/s (or 9.4×10^{-6} m/d, assuming a water density of 0.92 g/cm^3 at 222 K and no salinity). At this evaporation rate, discharges as low as 0.6 m^3/s could maintain this lake level (though higher discharges would certainly be necessary to fill a lake of this size). We have not found geomorphic evidence for or against a frozen surface on the proposed lakes.

A typical assessment of the runoff needed to build a depositional feature like the Pancake delta is to assume a rock to water ratio [e.g., *Mangold et al*., 2012b]. While rock/water ratios vary by orders of magnitude and depend on grain size and climate characteristics, a survey of terrestrial rivers by *Syvitski et al*. [2003] shows that the log transformed rock/water ratio yields a roughly Gaussian curve with a mean value of 0.0001 ± 0.00008 [*Palucis et al*., 2014]. For the volume of sediment comprising the Pancake delta (14 km^3), this would suggest that 140,000 km^3 of water runoff would have been needed, roughly 26 times the volume of the proposed lake. Using our steady state calculated discharge of 1.5 to 20 km^3/Earth year to maintain the lake and assuming that nearly all the water that kept the lake full came from erosion of Farah Vallis, a rock/water ratio of 0.0001 yields 1.5×10^{-4} to 2×10^{-3} km^3/Earth year of sediment transported. For the amount of sediment contained within the Pancake delta plus its associated plains (i.e., 20 km^3), it would take ~130,000 to 10,000 Earth years to build the Pancake delta while holding the water level constant. Obliquity cycles on Mars, which exert strong control on the climate system by altering the latitudinal variation of solar insolation (and hence affect ground temperatures, the size and location of dust storms, and the planetary distribution of volatiles [*Toon et al*., 1980; *Mellon and Jakosky*, 1995]), are thought to oscillate on timescales of ~1.2×10^5 years [*Ward*, 1974].

Due to the lack of definable channels on the Farah Vallis delta deposit, it is difficult to determine formative discharges during the time of delta building, but discharges ranging from 30 to 401 m^3/s (0.95 to 13 km^3/Earth year) would be needed to maintain a steady state lake level for the corresponding Farah Vallis lake stand (assuming losses to evaporation only). For the Dulce Vallis lake stand, discharges ranging from 25 to 334 m^3/s (0.75 to 10.5 km^3/Earth year) would be needed to maintain a steady state lake level (assuming loses to evaporation only). As water was likely sourced from multiple locations around Gale to maintain the two lower lake stands in Gale (as evidenced by multiple deltas defining the Farah Vallis and Dulce Vallis stands and the numerous crater wall gullies), it is difficult to estimate how long these stands persisted for based on the volumes of individual delta deposits. For the Dulce Vallis catchment, however, if the volume of sediment comprising the Dulce Vallis delta deposits (1.5 km^3) were deposited fluvially, then 15,000 km^3 of water

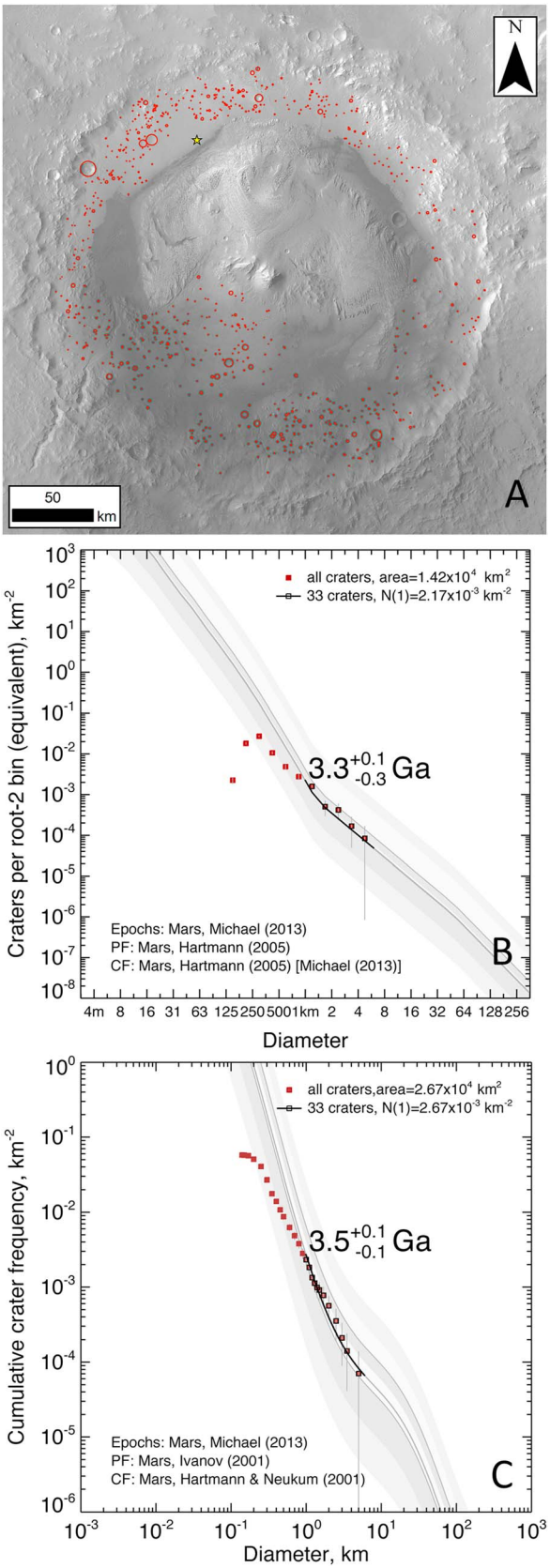

runoff would have been needed. For a drainage area of 450 km^2, that equates to 33 km of water. If the lake lasted less than 1000 years, runoffs of 33 m/yr would be needed, which is too high for even the wettest places on Earth. It is likely that these two lower lake stands lasted >1000 years.

6. Timing of Hydrogeomorphic Events in Gale Crater

6.1. Gale Impact and Mount Sharp Formation

Thomson et al. [2011] proposed that the impact age for Gale, based on crater counts in the surrounding ejecta and superposition relationships, lays at the Noachian-Hesperian boundary at ~3.6 to ~3.8 Ga. Some uncertainty in this age range is due to the occurrence of a few large craters for which it is not clear if they predate or postdate the Gale impact. They also counted craters on the crater floor and wall and concluded that the floor/wall were Early Hesperian age (their Figures 12c and 12d). We independently performed a crater count across the floor and wall of Gale (covering an area of 14,200 km^2 and mapping 819 craters) (Figure 20a) and found that craters greater than 1 km in diameter (33 craters), which perhaps are less likely to be affected by erosion and infilling and thus may best retain information about the minimum surface age of the floor of Gale [*Palucis*, 2014], fell on the 3.3 Ga isochron (Figure 20b) for the *Hartmann* [2005] system and on the 3.5 isochron for the *Ivanov* [2001]/*Hartmann and Neukum* [2001] system (Figure 20c). While we are proposing that large lakes occupied Gale for significant periods of time, our maximum estimate of lake duration for the largest lake stand (i.e., the Pancake Lake stand) is ~10^5 years, which

Figure 20. (a) Crater count map with a CTX mosaic underlain. (b) Crater count data for the wall and floor for all of Gale (area ~14,000 km^2) are shown on a *Hartmann* [2005] plot. All mapped crater sizes are plotted using root-2 binning, and there have been no resurfacing corrections. Craters >1 km in diameter fall approximately on the 3.3 Ga isochron. (c) The same data from Figure 20b are plotted on a cumulative frequency plot (pseudo log binning and again no resurfacing corrections). Craters >1 km in diameter fall approximately on the 3.5 Ga isochron in this system.

is still a small fraction of the total time that Gale's floor has been exposed to cratering; thus, these ages are unlikely to be affected by the lakes themselves. Therefore, based on these counts of Gale's floor and walls, we suggest that deposition of Mount Sharp deposits and subsequent erosion to form the mound likely occurred early on, perhaps within the first ~0.1 to ~0.5 Ga of Gale's history (i.e., 100 to 500 Ma for geomorphic work to occur).

6.2. Timing of Large Lakes

The deltaic features within Gale crater are small, ranging from several square kilometers (i.e., Entrance Canyon deposits) to 117 km^2 (i.e., Pancake delta), which precludes obtaining reliable absolute ages from crater counting [*Palucis and Dietrich*, 2014; *Warner et al*., 2015]. If we treat Gale's floor as a single "unit," however, then one possible interpretation is that most of the major depositional and geomorphic evolution (i.e., deposition and erosion to form the mound and deposition of the delta/fans) ended by ~3.3 to ~3.5 Ga and since that time most modifications have been due to wind erosion. *Fassett and Head* [2008a] also dated valley systems around Gale (including the Gale tributaries) and found a best fit age of Late Noachian/Early Hesperian, with error bars to Late Noachian to Late Hesperian, which supports that the incision of Farah Vallis and the timing of large lakes in Gale could have occurred relatively early on in Gale's history.

6.3. Timing of Fan Construction

For the Peace Vallis fan (~80 km^2), *Grant et al*. [2014] concluded that the upper portion of the fan must be Amazonian in age based on craters 90 to 150 m in diameter, but the fan is too small to have confidence in an absolute age derived from crater statistics. *Grant et al*. [2014] propose that the crater wall to the east of the fan (their CF1 and CF2, with areas of 307 and 236 km^2, respectively, and still relatively small areas) retains craters >400 m (12 craters for CF1 and 7 for CF2), suggesting an age of 3.2 to 3.3 Ga. In our analysis, we find that craters less than 1 km have likely been affected by erosion and infilling, which could mean that either Aeolis Palus (the plain between Gale's northern rim wall and Aeolis Mons) is more resistant to erosion and infilling compared to other regions of Gale's floor or that due to the small area of Aeolis Palus [*Warner et al*., 2015], these craters simply appear to be unaffected by erosion and infilling processes. Regardless, the age of Aeolis Palus is consistent with minimum surface ages derived from our 14,200 km^2 count area (though our crater size range is much less likely to have been affected by erosion and infilling). While it is possible that the Peace Vallis fan is younger than ~3.2 to 3.4 Ga, *Grant et al*. [2014] in arriving at that proposal disregarded a large crater on the upper portion of the fan (~760 m in diameter) under the assumption that it was part of the crater fill unit to the east. *Palucis* [2014] showed that the morphologic evidence points to the crater postdating the fan, and therefore, the fan would have formed early on in Gale's history. Other dated alluvial fans on Mars from cratering statistics range from the middle to late Hesperian to the Amazonian [*Grant and Wilson*, 2011, 2012; *Mangold et al*., 2012a, 2012b; *Morgan et al*., 2014], but in almost all of these cases, the fans are <1000 km^2 in size, so fan formation timing remains uncertain [e.g., *Warner et al*., 2015].

7. Discussion

7.1. Was Gale Connected to a Global Ocean?

Di Achille and Hynek [2010a, 2010b] identified four deltas within 260 km of Gale crater (two to the west and two to the east of Gale) that border the crustal dichotomy and would require an ocean (as the deltas are not confined within craters). The average elevation of these delta fronts is −2448 m. Topographic analysis of Gale crater shows that water levels higher than −2500 m would breach a roughly 22 km wide topographic corridor slightly beyond the northern rim. While this suggests the possibility that Gale was once connected to a northern ocean, there is no evidence of channel inflow or outflow across the topographic breach.

7.2. Comparisons With Other Proposed Hydrogeomorphic Histories for Gale

Several other alternative lake histories for Gale have been proposed in the literature, which differ some from the timeline presented here. *Pelkey and Jakosky* [2002], using Thermal Emission Imaging System (THEMIS) data, claim that the valleys rimming Gale Crater would postdate any large lake in Gale since they extend to the crater floor, but our analysis shows that these gully features terminate at two of our hypothesized shorelines (Dulce Vallis lake stand and Farah Vallis lake stand). *Irwin et al*. [2005] suggest that post-impact there was a brief reactivation of the highland valley networks resulting in the breach of Gale's rim, the dissection of Mount Sharp, the formation of gullies, and the deposition of fans and deltas. Mount Sharp is posited to have

formed prior to this time. While we are in general agreement with this model, improved imagery and topography allows for a more detailed timeline of events proposed here. *Anderson and Bell* [2010] suggest a lacustrine origin for the rocks comprising lower Mount Sharp, following *Malin and Edgett* [2000] and supported by *Grotzinger et al*. [2015], who suggest based on rover observations that the lower 75 to 250 m of the mound is lacustrine but do not make mention of any large lakes after Mount Sharp reached its current topographic form. They also examined the Entrance Canyon and its deposits (which they call the "fan-shaped unit") and suggest that material from the mound eroded and deposited as an alluvial fan atop what they refer to as the "mound-skirting material," which they describe as being pitted, mesaforming, and having parallel ridges at times. This is mapped in Figure 14 (numbered 5) as our broad, nearly uniform sloping plain. Figure 35 in *Anderson and Bell* [2010] propose that a single fan was constructed across the mound-skirting material and then was subsequently eroded back to the current outcrop pattern. The observed transitions between different units within the Entrance Canyon deposits, as well as the correspondence between the elevation of deposit 3's front (Entrance Canyon deposit #3, Figure 11) with the Dulce Vallis DD1 delta front and the coarse nature of the deposits (which might be difficult to erode by aeolian processes), point to multiple stages of deposition, some into a standing body of water (as opposed to a single deposit that formed subaerially and eroded back). Rover observations can hopefully distinguish between these two hypotheses in the future. If the Entrance Canyon deposits are an alluvial fan of predominately fluvial origin that has eroded back, we might expect to see moderately to well-sorted sandstone beds (perhaps normally graded with gravels deposited at the base of ephemeral channels), cross stratification associated with migrating bedforms, laterally extensive deposits deposited by sheet flows or braided river deposits, average grain sizes increasing as the rover traverses upslope, and evidence of erosional remnants where the deposit has since been eroded. If the deposits are the result of repeated debris flows entering a rising lake, we might expect to see poorly sorted matrix-supported beds (e.g., diamictites) that are approximately of uniform thickness but limited in lateral extent, a lack of stratification of the deposits, steeply dipping foresets where the flows entered a lake, lobate and/or levee deposits on the deltaic plain, and possibly Bouma and/or Lowe's sequences [*Cojan and Renard*, 2002].

Le Deit et al. [2013] noted various features in Gale that suggest directly or indirectly the presence of a lake (including what we have labeled as the lower Dulce delta (DD1)). They then proposed that a paleolake likely occurred within the range of −4450 and −3700 m. This range brackets (but does not match) two of the distinct lake stands we have found but omits the highest lake stand associated with Farah Vallis erosion and the formation of the Pancake delta at −3280 m. Our analysis also captures a complex lake history and suggests a shift in source water from large-scale northward drainage at the Pancake delta formation time to more local sources in subsequent lake stands (see below). They propose (their Figure 22) that a lake could have existed into the Late Hesperian and that fluvial processes could have resurfaced portions of Gale's floor into the Amazonian. We could find no definitive evidence to extend significant hydrologic activity beyond ~3.3 to 3.5 Ga.

As we mentioned previously, several authors have raised the possibility of frozen lakes and/or permafrost features within Gale [e.g., *Le Deit et al*., 2013; *Fairen et al*., 2014]. While it is possible that permafrost played some role at Gale, we do not observe strong evidence for features one might expect (i.e., pingos, gelifluction or solifluction lobes, rock glaciers, eskers, or stony patterned ground). It is also difficult to discern within the geomorphology whether or not the lake would have had an ice cover, though the apparent lack of wind wave influence on delta development, assuming the conditions allowed for wave development [*Banfield et al*., 2015], supports an ice cover hypothesis.

7.3. Sources of Water

Di Achille and Hynek [2010a, 2010b] and *Irwin et al*. [2005] identified several locations regional to Gale (within a ~600 km radius) where deep canyons breach a crater rim or the edge of a block of the dichotomy. In most of these cases the channels enter from the south to southwest, in the direction of the mean topographic gradient, just as Farah Vallis does. Our extended survey of this region (Figure S8 and Table S4) shows that there are 23 breach locations, and in 18 of these cases the steep canyons terminate in arcuate-shaped deposits, likely deltas or fans. This suggests that at least at the time of Farah Vallis' incision there was regional hydrologic activity resulting in large volumes of water flowing downslope from the south to the dichotomy and breaching craters from the south but not overflowing them.

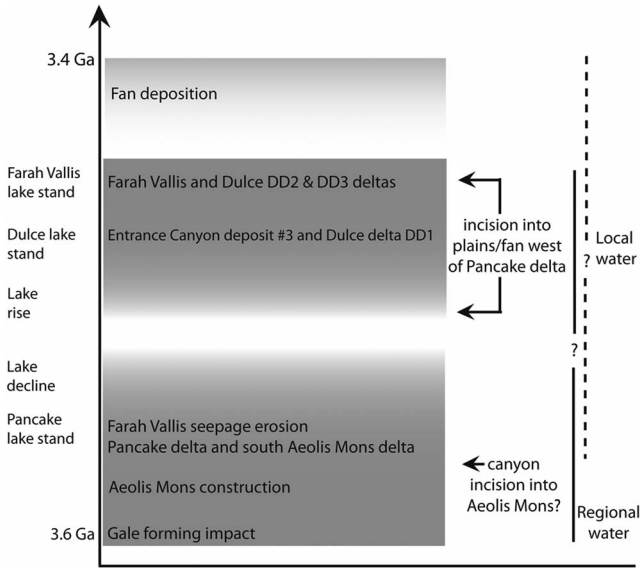

Figure 21. Our hypothesized sequence and relative timing of large lakes in Gale, which perhaps ended by 3.3 to 3.5 Ga; the likely water sources (distal via inputs from the south through Farah Vallis versus local via runoff from precipitation or snowmelt) and amounts of water (dark grey shading corresponds to a wet Gale, while light grey to white indicates drier periods) are also indicated.

Gale is unique, however, in that its internal dynamics, as recorded by multiple lake levels and smaller incised valleys (as mapped by *Anderson and Bell* [2010]), are not seen in any other craters in the region (~600 km radius). The nearest craters of comparable size are larger or older and more infilled, but they still expose ~1 km of inner crater wall, on which no relatively fresh incised valleys are observed. This suggests that local hydrologic processes were also important at Gale, in addition to regional water inputs (from the south). The observation that local incised valleys (gullies) terminate at the second and third lake stands is an indicator that local water inputs, at times of lake presence, became more important over time (Figure 21). *Kite et al.* [2011] propose, based on modeling, that water loses from a crater bound lake $\geq 10^3$ km^2 can produce intense localized precipitation (as snow) adjacent to the crater. As all of the large lakes within Gale are on the order of 3×10^3 km^2 or greater, it is possible, as *Kite et al.* [2011] suggested elsewhere, that evaporation from these lakes is responsible for setting up a hydrologic system at Gale. If fan formation occurred after these lakes stands, however, then local precipitation occurred independently of lakes at Gale as well, further shifting the relative water source from regional to local inputs (Figure 21). Based on the analysis in *Palucis et al.* [2014], building the Peace Vallis fan required more than 600 m of runoff, perhaps as much as 6 km, indicating the need for a hydrologic cycle that persisted for an extended period but was not intense enough to form a deep lake in Gale.

Both groundwater and surface water runoff have been considered to be possible water sources for Martian valley networks [*Malin and Carr*, 1999; *Malin and Edgett*, 2000; *Fassett and Head*, 2008b; *Goldspiel and Squyres*, 2011]. For Farah Vallis, *Irwin et al.* [2005] observed that the canyon is blocked from the upslope channel network by the Gale ejecta blanket. As Farah Vallis is not connected to the upslope drainage network to the south we hypothesize that regional groundwater flow from the south may have contributed significant amounts of water to Gale Crater. Alternatively, *Irwin et al.* [2005] and *Fassett and Head* [2008b] both argue that crater lakes to the south may have supplied water to Gale, as evidenced by their outlet breaches, but this runoff would have needed to infiltrate the subsurface, as Gale's ejecta blanket blocks Farah Vallis from receiving direct runoff from the south. As observed by *Fassett and Head* [2008b], there is a small basin at the headwaters of Farah Vallis that could have stored ponded water from the south and supplied the runoff needed to incise Farah Vallis, but this basin is small relative to the volumes of water needed to create and maintain the lakes hypothesized here, arguing for groundwater inputs from the south.

The source channels for the Dulce delta deposits, South fan, and Peace Vallis fan are visible and do not suggest a groundwater origin (as argued by *Palucis et al.* [2014]). Furthermore, the numerous incised valleys (gullies) that originate high on the crater wall (and not from distinct seepage points or alcoves) suggest local precipitation in Gale. It is possible, however, that some of the lake infilling during these hydrogeomorphic events could have been derived from regional groundwater at depth, while most of the water driving incision of valleys and delta and fan formation (both from the crater rim and mound) is derived from precipitation and runoff at the surface.

7.4. Implications for Gale and Martian Climate

Large volumes of water associated with these lake stands may have passed through or covered the sediments encountered by *Curiosity*, and our lake level sequencing suggests that most of the sediments the rover

has and will encounter experienced at least a few cycles of drying and wetting. The small deltaic deposits exiting canyons around Mount Sharp also imply that the mound experienced cycles of precipitation and runoff.

The sediment and water budgets of the deposits and associated lakes suggest that the hydrologic activity likely lasted at least thousands of years. Three distinct lake stands have been detected, but the interval of time between the lake stands is unknown. Global climate models show that snow accumulation and melting is possible in the equatorial highlands of Mars [e.g., *Wordsworth et al.*, 2013; *Kite et al.*, 2013], and snowmelt rates up to 3 mm/h are possible [*Kite et al.*, 2013]. These melt rates are adequate to drive even our highest estimated steady state discharges. It appears that these regional climatic events switched on and off suddenly, as we do not observe incision or gullying into most of the deltaic deposits. *Moore and Howard* [2005] reached a similar conclusion regarding large Noachian-Hesperian alluvial fans, where the lack of fan-head trenching and an absence in shifting of depositional centers indicate a rapid cessation of hydrologic activity. Even the small Peace Vallis fan (~80 km^2) required significant volumes of water, far beyond that which could be stored as a single snow pack. A sustained full hydrologic cycle is necessary to explain the deposits, geomorphology, and lake stands in Gale Crater.

8. Conclusions

After Aeolis Mons reached a state close to its current topographic form in Gale crater, at least three distinct lake high stands developed. The largest lake entirely within Gale is defined by the Pancake delta lake stand at −3280 m. The source of sediment and water was Farah Vallis. The Pancake lake stand would have been on average ~700 m deep and could have persisted for 10,000 to 130,000 Earth years. Near Gale, 18 other craters have short, deep canyons similar to Farah Vallis crossing their southern rims. This suggests that the hydrogeomorphic event that eroded Farah Vallis and led to lake formation was driven by regional water, perhaps groundwater, delivered from the south.

The highest lake level then dropped or completely evaporated before it rose to and then sustained a constant level at −3980 m (defined best by the Dulce delta DD1 deposit). The Dulce Vallis lake was on average ~300 m deep and likely lasted thousands of years. The lake then rose again to the Farah Vallis stand at −3780 m. The Farah Vallis lake, defined best by the Farah Vallis delta, was about 400 m deep and would have persisted for 18,000 to 240,000 Earth years. Gullies lining the northern crater rim and fan/deltas from Mount Sharp terminate at these two later lake stands. This suggests that the water source for hydrogeomophic change shifted from regional during the Pancake lake stand to more local precipitation in the later events. Taking the minimum formation times for each of these lacustrine phases suggests that lakes were intermittently present in Gale crater over at least a cumulative time span of 30,000 Earth years. The Peace Vallis fan is located at an elevation below all three of these large lakes. This low elevation, the lack of shorelines cutting it, its small size, and its generally strong topographic preservation all suggest that the Peace Vallis fan developed after these large lakes. The timing of Peace Vallis cannot be resolved by crater counting due to its small size.

As lake levels in Gale decreased, the low area immediately adjacent to the Curiosity landing site would have been one of the last areas to dry out, possibly contributing to shallow localized lake formation along the floor of the crater. All of the deposits that *Curiosity* has examined would have been subject to burial under deep lakes followed by desaturation.

The amount of water needed to produce the sediments from the distinct gullies in the well-defined watersheds of Dulce Vallis and Peace Vallis is equivalent to roughly 6 to 33 km of runoff (volume of water over catchment area). Hence, even for the smaller lakes and fan construction period, there would need to be a sustained hydrologic cycle. The identification of multiple distinct lake stands, the relatively large runoff volumes needed, and the apparent shift from a regional to more local water source point to climatic conditions in which an active hydrologic cycle perhaps operated intermittently but progressively diminished until hydrogeomorphic activity essentially ceased. This all occurred after Mount Sharp reached its current topographic form but may still have been within the first several hundred million years after the Gale impact.

Acknowledgments

This research was conducted for the Jet Propulsion Laboratory, California Institute of Technology, under a contract with NASA under the Mars Program Office. We would like to thank Alan Howard, the entire MSL team and especially John Grotzinger and Michael Malin for insightful discussions along the way. We greatly appreciate the comments and suggestions provided by Caleb Fassett, Nathalie Cabrol, and two anonymous reviewers. We also thank the teams responsible for the orbital data, namely, the HIRISE, CTX, and HRSC teams. We give a special thanks to Fred Calef, Malin Space Science Systems, and the USGS at Flagstaff, especially Annie Howington-Kraus and the Photogrammetry Guest Facility. All of the imagery used in this manuscript is freely available through the Planetary Data System (PDS) Imaging and Geoscience node or from GoogleEarth. The topographic data of Gale Crater/the MSL landing site that were derived from HIRISE, CTX, and HRSC were provided by the MSL mission and are cited properly and referred to in the reference list. A section of the MSL HiRISE base map and DEM (covering the rover traverse up to ~sol 1000) is scheduled for delivery to the PDS in March 2016, but all of the HIRISE, CTX, and HRSC imagery used by JPL/Caltech to make the MSL base maps are already available on the PDS. Any additional data (e.g., crater counts, ArcGIS mapping units, and CTX-derived topographic data of the southwestern portion of the crater made by MCP) may be obtained directly from MCP (mpalucis@caltech.edu).

References

Anderson, R. B., and J. F. Bell III (2010), Geologic mapping and characterization of Gale crater and implications for its potential as a Mars Science Laboratory landing site, *Mars J.*, *5*, 76–128, doi:10.1555/mars.2010.0004.

Ansan, V., and N. Mangold (2013), 3D morphometry of valley networks on Mars from HRSC/MEX DEMs: Implications for climatic evolution through time, *J. Geophys. Res. Planets*, *118*, 1873–1894, doi:10.1002/jgre.20117.

Banfield, D., M. Donelan, and L. Cavaleri (2015), Winds, waves, and shorelines from ancient Martian seas, *Icarus*, *250*, 368–383, doi:10.1016/j.icarus.2014.12.001.
Cabrol, N. A., and E. A. Grin (1999), Distribution, classification, and ages of Martian impact crater lakes, *Icarus*, *142*(1), 160–172, doi:10.1006/icar.1999.6191.
Cabrol, N. A., and E. A. Grin (Eds.) (2010), *Lakes on Mars*, Elsevier, Amsterdam, Netherlands.
Cabrol, N. A., E. A. Grin, H. E. Newsom, R. Landheim, and C. P. McKay (1999), Hydrogeologic evolution of Gale crater and its relevance to the exobiological exploration of Mars, *Icarus*, *139*(2), 235–245, doi:10.1006/icar.1999.6099.
Cojan, I., and M. Renard (2002), *Sedimentology*, CRC Press, Paris, France.
Craddock R. A., and A. D. Howard (2002), The case for rainfall on a warm, wet early Mars, *J. Geophys. Res.*, *107*(E11), 5111, doi:10.1029/2001JE001505.
Di Achille, G., and B. M. Hynek (2010a), Ancient ocean on Mars supported by global distribution of deltas and valleys, *Nat. Geosci.*, *3*(7), 459–463, doi:10.1038/NGEO891.
Di Achille, G., and B. M. Hynek (2010b), Deltas and valley networks on Mars: Implications for a global hydrosphere, in *Lakes on Mars*, edited by N. Cabrol and E. Grin, Chap. 8, Elsevier, New York.
Dietrich, W. E., T. Parker, D. Y. Sumner, A. Hayes, M. C. Palucis, R. M. E. Williams, F. Calef, and the MSL team (2013), Topographic evidence for Lakes in Gale crater, Lunar and Planetary Sci. Conf. XLIV, Abstract 1844.
Dietrich, W. E., M. C. Palucis, T. Parker, D. Rubin, M. A. de Pablo, D. Z. Oehler, and N. T. Bridges (2014), Looking towards Curiosity's canyon path: A 4 km sequence of gully, debris deposits, and fan/deltas which are bordered by a sloping bedform-capped plain and crossed by lake shorelines, Lunar and Planetary Sci. Conf. XLV, Abstract 1684.
Fairen, A. G., et al. (2014), A cold hydrological system in Gale crater, Mars, *Planet. Space Sci.*, *93–94*, 101–118, doi:10.1016/j.pss.2014.03.002.
Fassett, C. I., and J. W. Head (2008a), The timing of Martian valley network activity: Constraints from buffered crater counting, *Icarus*, *195*(1), 61–89, doi:10.1016/j.icarus.2007.12.009.
Fassett, C. I., and J. W. Head (2008b), Valley network-fed, open-basin lakes on Mars: Distribution and implications for Noachian surface and subsurface hydrology, *Icarus*, *198*, 37–56, doi:10.1016/j.icarus.2008.06.016.
Gilbert, G. K. (1890), Lake Bonneville, U.S. Geological Survey Monograph, Vol. I, 438 p.
Goldspiel, J. M., and S. W. Squyres (2011), Groundwater discharge and gully formation on Martian slopes, *Icarus*, *211*(1), 238–258, doi:10.1016/j.icarus.2010.10.008.
Golombek, M. P., et al. (2012), Selection of the Mars Science Laboratory Landing Site, *Space Sci. Rev.*, doi:10.1007/s11214-012-9916-y.
Golombek, M. P., N. H. Warner, V. Ganti, M. P. Lamb, T. J. Parker, R. L. Fergason, and R. Sullivan (2014), Small crater modification on Meridiani Planum and implications for erosion rates and climate change on Mars, *J. Geophys. Res. Planets*, *119*, 2522–2547, doi:10.1002/2014JE004658.
Grant, J. A., and S. A. Wilson (2011), Late alluvial fan formation in southern Margaritifer Terra, Mars, *Geophys. Res. Lett.*, *38*, L08201, doi:10.1029/2011GL046844.
Grant, J. A., and S. A. Wilson (2012), A possible synoptic source of water for alluvial fan formation in Southern Margaritifer Terra, Mars, *Planet. Space Sci.*, *72*(1), 44–52.
Grant, J. A., S. A. Wilson, N. Mangold, F. Calef, and J. P. Grotzinger (2014), The timing of fluvial activity in Gale crater, Mars, *Icarus*, *41*(4), 1142–1149, doi:10.1002/2013GL058909.
Grotzinger, J. P., et al. (2014), A habitable fluvio-lacustrine environment at Yellowknife Bay, Gale crater, Mars, *Science*, *343*, doi:10.1126/science.1242777.
Grotzinger, J. P., et al. (2015), Deposition, exhumation, and paleoclimate of an ancient lake deposit, Gale crater, Mars, *Science*, *350*(6257), doi:10.1126/science.aac7575.
Hartmann, W. K. (2005), Martian cratering 8: Isochron refinement and the chronology of Mars, *Icarus*, *174*, 294–320.
Hartmann, W. K., and G. Neukum (2001), Cratering chronology and the evolution of Mars, *Space Sci. Rev.*, 165–194.
Head, J. W., and S. Pratt (2001), Extensive Herperian-aged south polar ice sheet on Mars: Evidence for massive melting and retreat, and lateral flow and ponding of meltwater, *J. Geophys. Res.*, *106*(E6), 12,275–12,299, doi:10.1029/2000JE001359.
Hecht, M. H. (2002), Metastability of liquid water on Mars, *Icarus*, *156*(2), 373–386, doi:10.1006/icar.2001.6794.
Howard, A. D., J. M. Moore, and R. P. Irwin (2005), An intense terminal epoch of widespread fluvial activity on early Mars: 1. Valley network incision and associated deposits, *J. Geophys. Res.*, *110*, E12S14, doi:10.1029/2005JE002459.
Hynek, B. M., M. Breach, and M. R. T. Hoke (2010), Updated global map of Martian valley networks and implications for climate and hydrologic processes, *J. Geophys. Res.*, *115*, E09008, doi:10.1029/2009JE003548.
Ingersoll, A. (1970), Mars: Occurrence of liquid water, *Science*, *168*(3934), 972–973, doi:10.1126/science.168.3934.972.
Irwin, R. P., A. D. Howard, R. A. Craddock, and J. M. Moore (2005), An intense terminal epoch of widespread fluvial activity on early Mars: 2. Increased runoff and paleolake development, *J. Geophys. Res.*, *110*, E12S15, doi:10.1029/2005JE002460.
Ivanov, B. A. (2001), Mars/Moon cratering rate ratio estimates, in chronology and evolution of Mars, in *Proceedings of an ISSI Workshop, 10–14 April 2000, Bern, Switzerland*, pp. 87–104, Springer, Netherlands, doi:10.1007/978-94-017-1035-0_4.
Kite, E. S., T. I. Michaels, S. Rafkin, M. Manga, and W. E. Dietrich (2011), Localized precipitation and runoff on Mars, *Icarus*, *116*(E7), doi:10.1029/2010JE003783.
Kite, E. S., I. Harvey, M. A. Kahre, M. J. Wolff, and M. Manga (2013), Seasonal melting and the formation of sedimentary rocks on Mars, with predictions for the Gale crater mound, *Icarus*, *223*, 131–210, doi:10.1016/j.icarus.2012.11.034.
Kneissl, T., S. van Gassalt, and G. Neukum (2011), Map-projection-independent crater size-frequency determination in GIS environments—New Software tool for ArcGIS, *Planet. Space Sci.*, *59*(11–12), 1243–1254, doi:10.1016/j.pss.2010.03.015.
Kraal, E. R., M. van Jijk, G. Postma, and M. G. Kleinhans (2008), Martian stepped-delta formation by rapid water release, *Nature*, *451*, 973–976, doi:10.1038/nature06615.
Kuznetz, L. H., and D. C. Gan (2002), On the existence and stability of liquid water on the surface of Mars today, *Astrobiology*, *2*(2), 183–195, doi:10.1089/15311070261092255.
Le Deit, L., E. Hauber, F. Fueten, M. Pondrelli, A. Rossi, and R. Jaumann (2013), Sequence of infilling events in Gale crater, Mars: Results from morphology, stratigraphy, and mineralogy, *J. Geophys. Res. Planets*, *118*, 2439–2473, doi:10.1002/2012JE004322.
Malin, M. C., and M. H. Carr (1999), Groundwater formation of Martian valleys, *Nature*, *397*, 589–591, doi:10.1038/17551.
Malin, M. C., and K. S. Edgett (2000), Sedimentary rocks on early Mars, *Science*, *290*, 1927, doi:10.1126/science.290.5498.1927.
Mangold, N., S. Adeli, S. Conway, V. Ansan, and B. Langlais (2012a), A chronology of early Mars climatic evolution from impact crater degradation, *J. Geophys. Res.*, *117*, E04003, doi:10.1029/2011JE004005.
Mangold, N., E. S. Kite, M. G. Kleinhans, H. Newsom, V. Ansan, E. Hauber, E. Kraal, C. Quantin, and K. Tanaka (2012b), The origin and timing of fluvial activity at Eberswalde crater, Mars, *Icarus*, *220*(2), 530–551, doi:10.1016/j.icarus.2012.05.026.

Mellon, M. T., and B. M. Jakosky (1995), The distribution and behavior of Martian ground ice during past and present epochs, *J. Geophys. Res.*, *100*(E6), 11,781–11,799, doi:10.1029/95JE01027.
Michael, G. G., and G. Neukum (2010), Planetary surface dating from crater size-frequency distribution measurements: Partial resurfacing events and statistical age uncertainty, *Earth Planet. Sci. Lett.*, doi:10.1016/j.epsl.2009.12.041.
Milliken, R. E., J. P. Grotzinger, and B. J. Thomson (2010), Paleoclimate of Mars as captured by the stratigraphic record in Gale crater, *Geophys. Res. Lett.*, *37*, L04201, doi:10.1029/2009GL041870.
Milliken, R. E., R. C. Ewing, W. W. Fischer, and J. Hurowitz (2014), Wind-blown sandstones cemented by sulfate and clay minerals in Gale Crater, Mars, *Geophys. Res. Lett.*, *41*, 1149–1154, doi:10.1001/2013GL059097.
Moore, J. M., and A. D. Howard (2005), Large alluvial fans on Mars, *J. Geophys. Res.*, *110*, E04005, doi:10.1029/2004JE002352.
Moore, J. M., A. D. Howard, W. E. Dietrich, and P. M. Schenk (2003), Martian layered fluvial deposits: Implications for Noachian climate scenarios, *Geophys. Res. Lett.*, *30*(24), 2292, doi:10.1029/2003GL019002.
Morgan, A. M., A. D. Howard, D. E. Hobley, J. M. Moore, W. E. Dietrich, R. M. E. Williams, D. M. Burr, J. A. Grant, S. A. Wilson, and Y. Matsubara (2014), Sedimentology and climatic environment of alluvial fans in the Martian Saheki crater and a comparison with terrestrial fans in the Atacama Desert, *Icarus*, *229*, 131–156.
Muto, T., and R. Steel (2001), Autostepping during the transgressive growth of deltas: Results from flume experiments, *Geology*, *29*(9), 771–774.
Newsom, H. E., et al. (2014), Gale crater and impact processes—Observations during Curiosity's first 360 sols on Mars, *Icarus*, *249*, 108–128, doi:10.1016/j.icarus.2014.10.013.
Palucis, M. C. (2014), Using quantitative topographic analysis to understand the role of water on transport and deposition processes on crater walls, UC Berkeley Dissertation.
Palucis, M. C., and W. E. Dietrich (2014), A Model for Assessing Uncertainties Associated with Individual Crater Age Measurements for Small Areas ($<$ 1000 km2), LPI Contributions, 8th International Conference on Mars, Abstract 1295.
Palucis, M. C., W. E. Dietrich, A. G. Hayes, R. M. E. Williams, S. Gupta, N. Mangold, H. Newsom, C. Hardgrove, F. Calef, and D. Y. Sumner (2014), The origin and evolution of the Peace Vallis fan system that drains to the Curiosity landing area, Gale crater, Mars, *J. Geophys. Res. Planets*, *119*, 705–728, doi:10.1002/2013JE004583.
Pelkey, S. M., and B. M. Jakosky (2002), Surficial geologic surveys of Gale crater and Melas Chasma Mars: Integration of remote-sensing data, *Icarus*, *160*(2), 228–257, doi:10.1006/icar.2002.6978.
Pelkey, S. M., B. M. Jakosky, and P. R. Christensen (2004), Surficial properties in Gale crater, Mars, from Mars Odyssey THEMIS data, *Icarus*, *167*(2), 244–270, doi:10.1016/j.icarus.2003.09.013.
Sears, D. W., and J. D. Chittenden (2005), On laboratory simulation and the temperature dependence of the evaporation rate of brine on Mars, *Geophys. Res. Lett.*, *32*, L23203, doi:10.1029/2005GL024154.
Sears, D. W. G., and S. R. Moore (2005), On laboratory simulation and the evaporation rate of water on Mars, *Geophys. Res. Lett.*, *32*, L16202, doi:10.1029/2005GL023443.
Stock, J. E. (2013), Waters divided: A history of alluvial fan research and a view of its future, in *Treatise on Geomorphology*, edited by J. Shroder and E. Wohl, vol. 9, pp. 413–458, Academic Press, San Diego, Calif., Fluvial Geomorphology.
Syvitski, J. P. M., S. D. Peckham, R. Hilberman, and T. Mulder (2003), Predicting the terrestrial flux of sediment to the global ocean: A planetary perspective, *Sediment. Geol.*, *162*(1–2), 5–24, doi:10.1016/S0037-0738(03)00232-X.
Thomson, B. J., N. T. Bridges, R. Milliken, A. Baldridge, S. J. Hook, J. K. Crowley, G. M. Marion, C. R. de Souza, A. J. Brown, and C. M. Weitz (2011), Constraints on the origin and evolution of the layered mound in Gale crater, Mars using Mars Reconnaissance Orbiter data, *Icarus*, *214*(2), 413–432, doi:10.1016/j.icarus.2011.05.002.
Toon, O. B., J. B. Pollack, W. Ward, J. A. Burns, and K. Bilski (1980), The astronomical theory of climatic change on Mars, *Icarus*, *44*(3), 552–607, doi:10.1016/0019-1035(80)90130-X.
Vasavada, A. R., et al. (2014), Overview of the Mars Science Laboratory Mission: Earth to Bradbury Landing and Yellowknife Bay, *J. Geophys. Res. Planets*, *119*, 1134–1161, doi:10.1002/2014JE004622.
Wallace, D., and C. Sagan (1979), Evaporation of ice in planetary atmospheres: Ice-covered rivers on Mars, *Icarus*, *39*(3), 385–400, doi:10.1016/0019-1035(79)90148-9.
Ward, W. R. (1974), Climatic variations on Mars: 1. Astronomical theory of insolation, *J. Geophys. Res.*, *79*(24), 3375–3386, doi:10.1029/JC079i024p03375.
Warner, N. H., S. Gupta, J. R. Kim, J. P. Muller, L. L. Corre, J. Morley, S. Y. Lin, and C. McGonigle (2011), Constraints on the origin and evolution of Iani Chaos, Mars, *J. Geophys. Res.*, *116*, E06003, doi:10.1029/2010JE003787.
Warner, N. H., S. Gupta, F. Calef, P. Grindrod, N. Boll, and K. Goddard (2015), Minimum effective area for high resolution crater counting of Martian terrains, *Icarus*, *245*, 198–240, doi:10.1016/j.icarus.2014.09.024.
Williams, R. M. E., R. P. Irwin III, and J. R. Zimbelman (2009), Evaluation of paleohydrologic models for terrestrial inverted channels: Implications for application to Martian Sinuous Ridges, *Geomorphology*, *107*(3–4), 300–315, doi:10.1016/j.geomorph.2008.12.015.
Wordsworth, R., F. Forget, E. Millour, J. W. Head, J. B. Madeleine, and B. Charnay (2013), Global modeling of the early Martian climate under a denser CO2 atmosphere: Water cycle and ice evolution, *Icarus*, *222*(1), 1–19, doi:10.1016/j.icarus.2012.09.036.